Investigating Methods of Neutrinoless Double-Beta Decay Detection

Matthew Rose, Physics MSci
University College London
Supervisor: Dr R. Saakyan

March 22, 2007

Abstract

The Super-NEMO experiment is searching for $0\nu\beta\beta$ events to establish the nature of the neutrino (Majorana or Dirac) and place limits on the effective neutrino mass, as well as establishing the neutrino mass eigenstate hierarchy. To do this the energy resolution of the calorimeter used to find the energies of electrons emitted by $\beta\beta$ decay must be improved from 14-17%[1] to 7% at 1 MeV, by increasing the amount of photoelectrons entering the photomultiplier tubes (PMTs) of the calorimeter.

The precise wavelength spectra of the scintillators chosen for use in the calorimeter must be established using a spectrometer, and combined with the Quantum Efficiency of the PMTs in order to find the combination that will produce the maximum electrical signal upon detection of an electron with an energy in the $0\nu\beta\beta$ decay range. The energy resolution of the scintillators can then be measured using a β decay source and a PMT, and compared with predictions made using data from the manufacturers of both elements.

Four scintillator samples were studied - BC-404, BC-408 and BC-412, all PVT scintillators made by Bicron, and a polystyrene sample from Karkhov in the Ukraine, about which little was known. The measured wavelength spectra and the manufacturer's spectra did not correspond as well as expected. A shift towards longer wavelengths was observed, as well as the presence of unexpected shoulder regions. The energy resolutions achieved at 967 keV for the three Bicron scintillators were 7.8%, 8.2% and 10.4% respectively - the results for BC-404 and BC-408 are in close agreement with resolutions previously measured for the same scintillators with a different PMT[2], and also imply that an energy resolution of 7% at 1 MeV is obtainable. Either the use a different PMT chosen on the basis of the measured emission spectra of the scintillators, or the development of scintillator samples with emission spectra shifted towards shorter wavelengths should lead to an improvement in the energy resolution of the calorimeter.

Acknowledgements

Thanks must go to Matt Kauer and Dr. M. Lancaster for their help with all things related to computers and programming, and to Brian Anderson for his endless help and availability. I would also like to thank Dr. R. Saakyan for his patience, encouragement and enthusiasm for this project.

For helping me to find my feet in unfamiliar ground, and for their continuing support over the last four years, I owe a great debt of gratitude to Jack Brennan, Dominic da Costa, Tom Cherry, Josh Hayward, Anna Dejardin, Dara McCutcheon and everyone at Old Castle Farm.

Matthew Rose
March 22, 2007

Contents

List of Figures

List of Tables

1 Introduction

1.1 Amending the Standard Model

The Standard Model of particle physics states that all neutrinos must be left-handed (have negative helicity) and all anti-neutrinos must be right-handed (positive helicity), and therefore both must be exactly massless. Recent results from Super-Kamiokande (SK) and the Sudbury Neutrino Observatory (SNO) have called this model into question - these experiments have produced evidence for neutrino oscillations, and as such predict that neutrinos have non-zero mass, violating the Standard Model.

While this is indeed very significant, it does not answer the question of the nature of the neutrino. Unlike all the other fermions in the Standard Model, due to the fact that neutrinos have neutral charge it is possible that they may be Majorana particles, i.e their own anti-particles. If this is the case, then neutrinoless double beta decay ($0\nu\beta\beta$) is possible and an observation of a $0\nu\beta\beta$ event can be taken as confirmation of the Majorana nature of the neutrino.

1.2 What is $\beta\beta$ Decay?

Two Neutrino Double Beta Decay ($2\nu\beta\beta$) is the phenomenon whereby two neutrons simultaneously decay into two protons by emission of two β particles and two $\overline{\nu_e}$. This decay is shown in Equation 1 and Figure 1. Neutrinoless Double Beta Decay, or $0\nu\beta\beta$, is the simultaneous β decay of two neutrons by the simultaneous emmision of a $\overline{\nu_e}$ and absorption of a ν_e. It is a special case of $2\nu\beta\beta$ decay, only possible if the neutrino is found to be a Majorana Neutrino (ν_M) as shown in Equation 2 and Figure 2. In order to conserve helicity, the $\overline{\nu}_e$ must be right-handed, and the ν_e must be left-handed, meaning that the majorana neutrino must change helicity. This change is only possible if the ν_e has mass, as otherwise there exists no reference frame in which one can travel faster than the ν_e and observe a change in helicity.

$$2n \rightarrow 2p + 2\beta + 2\overline{\nu}_e \tag{1}$$

$$2n \rightarrow 2p + 2\beta \tag{2}$$

$$\begin{pmatrix} n \rightarrow p + \beta + \overline{\nu}_e \\ \nu_e + n \rightarrow p + \beta \\ \overline{\nu}_e \equiv \nu_e \equiv \nu_M \end{pmatrix}$$

There is currently a resurgence of interest in the detection of $0\nu\beta\beta$ decays, as results from SK and other sources have allowed a prediction to be

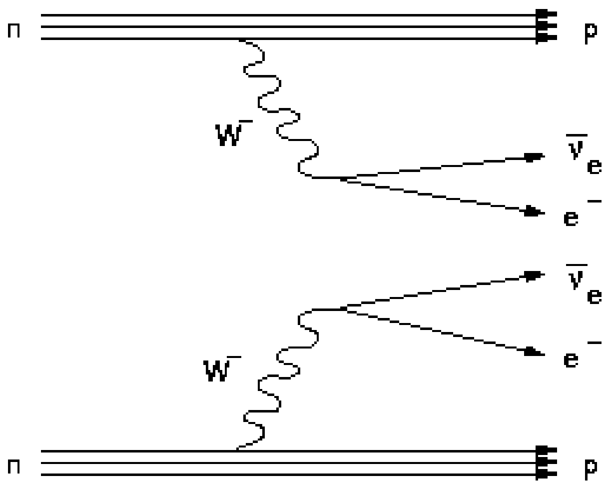

Figure 1: Feynman Diagram of $2\nu\beta\beta$ decay.

made about the mass of the neutrino. Neutrino oscillations depend on Δm^2, the difference squared between the two mass eigenstates that a neutrino is oscillating between, and by assuming that $\Delta m^2 \simeq 1.9 - 3.5 \times 10^{-3} eV^2$ with a best fit value of $2.8 \times 10^{-3} eV^2$ [5], and that one neutrino eigenstate has vanishing mass, one can easily estimate that the mass of the other is between 0.04 and 0.06eV. Current methods of $0\nu\beta\beta$ detection are not yet sensitive to energies in this range, but the new generation of $0\nu\beta\beta$ experiments aims to achieve this sensitivity. $0\nu\beta\beta$ events are extremely rare - $2\nu\beta\beta$ decay is the rarest weak decay permitted by the standard model, with a half-life of around $T^{2\nu}_{1/2} \simeq 1.4 \times 10^{21} yr$ for the decay shown in Equation 3, while the half-life of $0\nu\beta\beta$ decay as measured by Klapdor-Kleingrothaus [6] is of the order of $T^{0\nu}_{1/2} \simeq (0.08 - 3.5)10^{26} yr$ for the same decay [7], meaning that the predicted ratio of $2\nu\beta\beta$ to $0\nu\beta\beta$ events could be of the order of 10^6.

$$^{76}Ge \rightarrow ^{76} Se + 2e^- + (2\nu) \tag{3}$$

$$[T^{2\nu}_{1/2}]^{-1} = G_{2\nu} |\mathcal{M}_{2\nu}|^2 / log(2) \tag{4}$$

$$[T^{0\nu}_{1/2}]^{-1} = (\langle m_\nu \rangle / m_e)^2 G_{0\nu} |\mathcal{M}_{0\nu}|^2 / log(2) \tag{5}$$

The half-lives stated above are calculated using the formulae in Equations 4 and 5, where $\langle m_\nu \rangle$ is the effective neutrino mass and m_e, $\mathcal{M}_{0,2\nu}$ (the

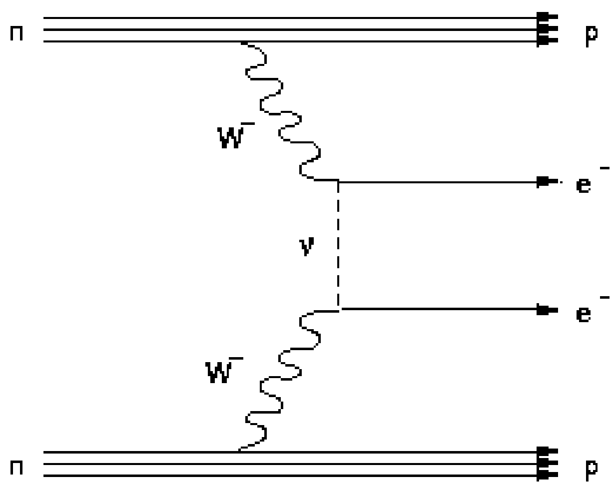

Figure 2: Feynman Diagram of $0\nu\beta\beta$ decay, where ν represents both ν_e and $\overline{\nu_e}$.

matrix element) and $G_{0,2\nu}$ (phase-space factor) are known/well calculated quantities, with $G_{2\nu} \propto Q_{\beta\beta}^{11}$ and $G_{0\nu} \propto Q_{\beta\beta}^{5}$. $Q_{\beta\beta}$ is the difference between the energies of the parent and daughter nuclei, and therefore is also the sum of the energies of the electrons emitted during $0\nu\beta\beta$ decay. In a three-neutrino oscillation model, the ν_e can be thought of as a superposition of the three neutrino mass eigenstates ν_1, ν_2 and ν_3, as in Equation 6 [1]. $\langle m_\nu \rangle$ can therefore be thought of as a superposition as well, also shown in Equation 7. An observation of $0\nu\beta\beta$ decay would place limits on this quantity, allowing the neutrino-mass hierarchy to be better understood - there are currently two experimental values for the mass difference squared, Δm^2_{sol} (from solar ν experiments, associated with $\nu_1 \rightarrow \nu_2$) and Δm^2_{atm} (from atmospheric ν experiments, associated with $\nu_2 \rightarrow \nu_3$), neither of which provide information about whether ν_3 is lighter or heavier than $\nu_{1,2}$. Detection of $0\nu\beta\beta$ events would place limits upon $T^{0\nu}_{1/2}$ and therefore also on $\langle m_\nu \rangle$ as well as giving information about the dependency of $\langle m_\nu \rangle$ on the lightest neutrino mass, and so demonstrate the mass hierarchy[2].

[1] U_{ei} is the neutrino mixing matrix, measured by neutrino oscillation experiments.
[2] For a more detailed treatment, see [8].

$$\nu_e = \sum_{i=1}^{3} U_{ei}\nu_i \tag{6}$$

$$\langle m_\nu \rangle = \sum_{i=1}^{3} U_{ei}^2 m_{\nu_i} \tag{7}$$

1.3 Super-NEMO - detecting $0\nu\beta\beta$ decays

The Super-NEMO project is the latest incarnation of the NEMO[3] Project, aiming to determine the fundamental nature of the neutrino, as well as discovering its mass scale. Super-NEMO is a progression from NEMO-III, a successful $\beta\beta$ decay experiment which has been running since February 2003 and has found strong agreement between simulated and measured $2\nu\beta\beta$ events, but has found no evidence for $0\nu\beta\beta$ decay[4] after 389 days of operation [10]. It is hoped that by increasing the amount of $\beta\beta$ source used (from 10 - 100kg) and by increasing the energy resolution compared to NEMO-III, Super-NEMO will find confirmed instances of $0\nu\beta\beta$ decay.

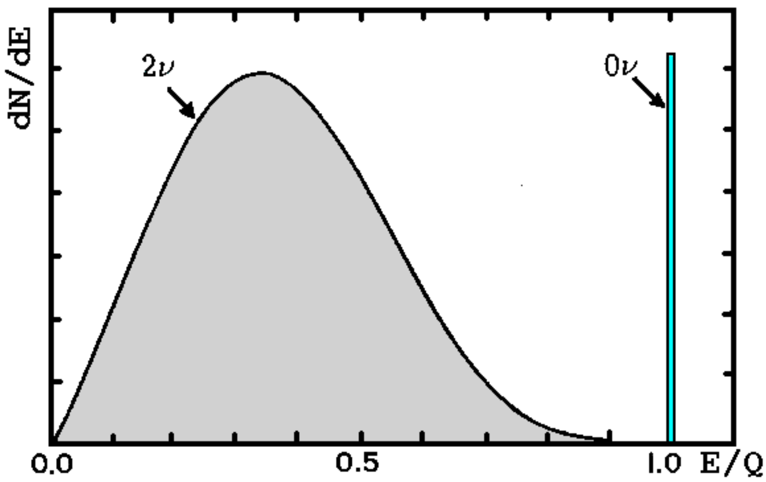

Figure 3: Calculated Spectra for ^{100}Mo $\beta\beta$ decays [11], showing $2\nu\beta\beta$ and $0\nu\beta\beta$ energy spectra

It is possible to predict the energy spectra of $2\nu\beta\beta$ and $0\nu\beta\beta$ through simulations, as shown in Figure 3, which can be seen to stop abruptly at

[3]**N**eutrino **E**ttore **M**ajorana **O**bservatory.

[4]It should be noted that while there is a claim for the the existence of a $0\nu\beta\beta$ event from the Heidelberg-Moscow collaboration[6], this result is controversial and has not yet been deemed conclusive[9]

$E \simeq 3034keV$, the $Q_{\beta\beta}$ value of ^{100}Mo. These calculated spectra show that $0\nu\beta\beta$ decay has a distinct energy signature from $2\nu\beta\beta$ decay, and as such should be relatively simple to identify. However, due to the rarity of the decay the predicted energy signature is tiny compared to that of $2\nu\beta\beta$ an approximation of which is shown in Figure 4. It is for this reason that the energy resolution of next generation $0\nu\beta\beta$ detection experiments must be better than that of those currently detecting $2\nu\beta\beta$ decays.

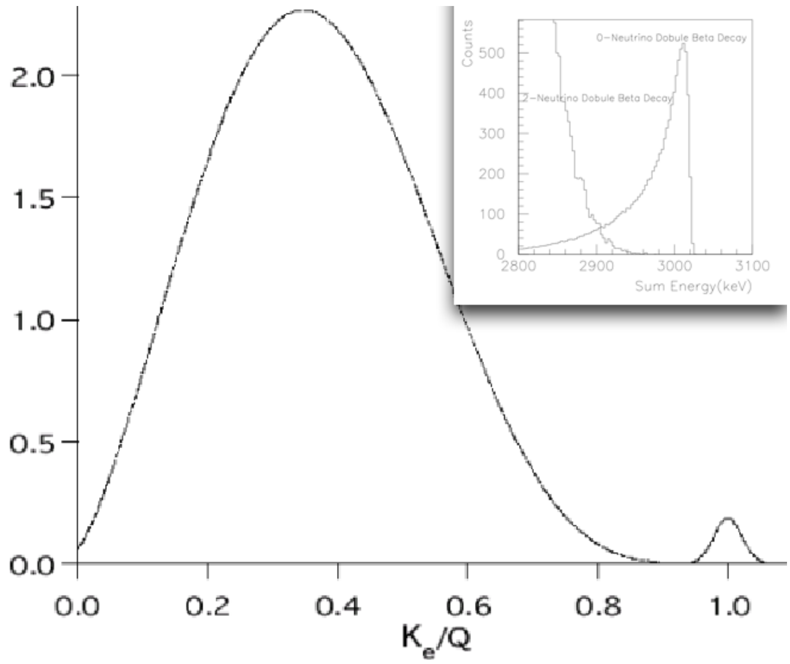

Figure 4: A schematic view of the sum energy spectra of $\beta\beta$ decays, with a simulated ^{100}Mo spectrum assuming a $2\nu\beta\beta$ to $0\nu\beta\beta$ ratio of 1:10^6 (insert) [7, 12].

A large problem with identification of $0\nu\beta\beta$ events is background radiation - the signature is so small that a zero-background detector must be constructed in order to stand any chance of detecting these rare events. Background radiation can be attributed to atmospheric muons entering the detector, trace amounts of Uranium and Thorium in the materials used to build the detector, and also to Radon gas in the Lab. Interference from such radiation can be reduced by building the detector underground to minimize atmospheric interference, by purifying the materials used in the detector (such as the wires, radioactive foils and so on), and by enclosing the detector in an 'Anti-Radon tent' capable of reducing the Radon activity by a factor of $\simeq 100$ compared to air in the Lab[5]. The energy ranges of all these background sources are known, so it is possible to further minimize their effects by the choice of the $\beta\beta$ source - inspection of the decay chains of ^{238}U and ^{232}Th reveals that there are only two β emitters with a Q_β value greater than 3MeV[6], meaning that these produce γ and β radiation energetic enough to resemble $0\nu\beta\beta$ events at 3MeV. Few nuclei exist for which $\beta\beta$ decay is energetically permitted, and it is of paramount importance to select a nucleus with a $Q_{\beta\beta}$ value higher than 2.6 MeV, the energy of most common background sources. Also, a high $Q_{\beta\beta}$ value will increase the phase-space factor $G_{0\nu}$ and therefore also the decay rate. The chosen source for Super-NEMO is Selenium, which decays as shown in Equation 8.

$$^{82}Se \rightarrow ^{82} Kr + 2e^- + (2\nu_e), Q_{\beta\beta} = 2995 \pm 6keV \tag{8}$$

2 Calorimeter Design

Figure 4 shows that there is a significant overlap between the two decays, and in order to separate $0\nu\beta\beta$ from $2\nu\beta\beta$ and background events a calorimeter capable of high energy resolution is required. The effect of higher energy resolution is to reduce the spread of energies for $2\nu\beta\beta$ and $0\nu\beta\beta$ events, therefore also reducing the overlap between the two energy spectra. The source foils within Super-NEMO will be surrounded by a tracking volume which provides three-dimensional tracks of charged particles, allowing their common vertex to be identified. The tracking volume is is then surrounded by a scintillator detector calorimeter similar in many ways to that used in NEMO-III[1]. This structure can be seen in Figure 5a. The calorimeter provides information about the energies and timing of emitted particles. The resolution of this calorimeter depends on the choice of plastic scintillator and photomultiplier tubes (PMTs) used (Arranged as shown in Figure 5b). The fractional energy resolution, $\frac{\Delta E}{E}$ of a detector at a certain energy E is shown in Equation 9. σ is the standard deviation of the energy spectrum, which is a poisson distribution[7]. Knowing this, it is possible to fit curves to measured spectra at known energies, and calculate σ and therefore $\frac{\Delta E}{E}$ of various scintillator and PMT combinations.

$$\frac{\Delta E}{E} = \frac{FWHM}{E} = \frac{\sqrt{8ln(2)}\sigma}{E} \simeq \frac{2.35\sigma}{E} \tag{9}$$

[5]Already in place on NEMO-III.[13]

[6]These are ^{214}Bi and ^{208}Tl, $Q_{\beta\beta} = 3.272$ and 5.001 MeV respectively.[14]

[7]This can be seen in Figures 3 and 4 above.

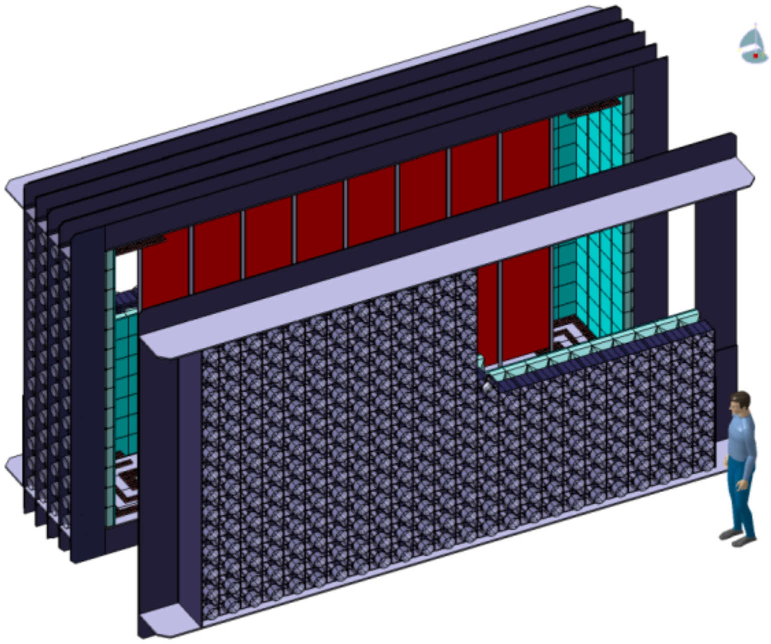

(a) A Super-NEMO sub-module, containing approximately 7kg of $\beta\beta$ source foil, surrounded by PMT & scintillator calorimeters.

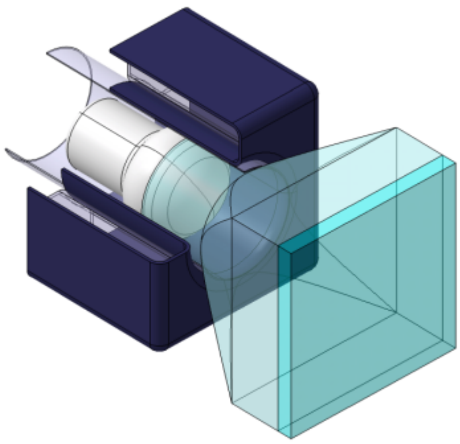

(b) Detail of a single PMT and scintillator.

Figure 5: Designs for a single Super-NEMO sub-module[15].

2.1 Scintillators

The calorimeter will consist of two walls of scintillators either side of the source foil (^{82}Se). These will measure the energies of charged particles and gammas produced by the foil, using a magnetic field to differentiate between electrons and positrons. The scintillator blocks will be covered in aluminized Mylar, to avoid any ambient light entering the blocks and also to maximize the light reflection inside the scintillator.

2.2 PMTs

The purpose of the PMT is to take the photon output of the scintillator and convert it into an electrical signal. Photons are converted to photoelectrons by absorption in a photocathode layer. The electrons are then pulled to a series of dynodes which amplify the electronic signal - typical PMTs can provide a gain of 10^6 compared to the original signal. Larger gain increases the precision of energy readings, as it becomes easier to discern particular energy signatures. The Quantum Efficiency (Q.E.) of a PMT is defined as the number of photoelectrons produced at the cathode over the number of photons entering the PMT, $Q.E. = \frac{N_\gamma}{N_{pe}}$. It is a function of the wavelength of the incident photons, which in turn depends on the choice and geometry of the scintillator used.

When a particle enters a scintillator and produces photons, the number of photons produced (N_γ) is proportional to the energy of the particle. N_{pe} is therefore also proportional to the energy of the incident particle. The distribution of N_{pe} is a poisson distribution, meaning that the standard deviation is the square root of the mean. Equation 10 shows that $\frac{\Delta E}{E}$ depends on the light output of the scintillator and the Q.E. of the PMT, and that to obtain an improvement in $\frac{\Delta E}{E}$ of a factor of 2, an increase of N_{pe} by a factor of 4 is required. This is why the matching of the wavelength of maximum emission of a scintillator with that of maximum Q.E. of a PMT is so important.

$$\sigma_{pe} = \sqrt{N_{pe}}$$

$$\frac{2.35\sigma}{E} \propto \frac{2.35\sqrt{N_{pe}}}{N_{pe}} = \frac{2.35}{\sqrt{N_{pe}}} \tag{10}$$

$$\frac{\Delta E}{E} \propto 1/\sqrt{N_{pe}}$$

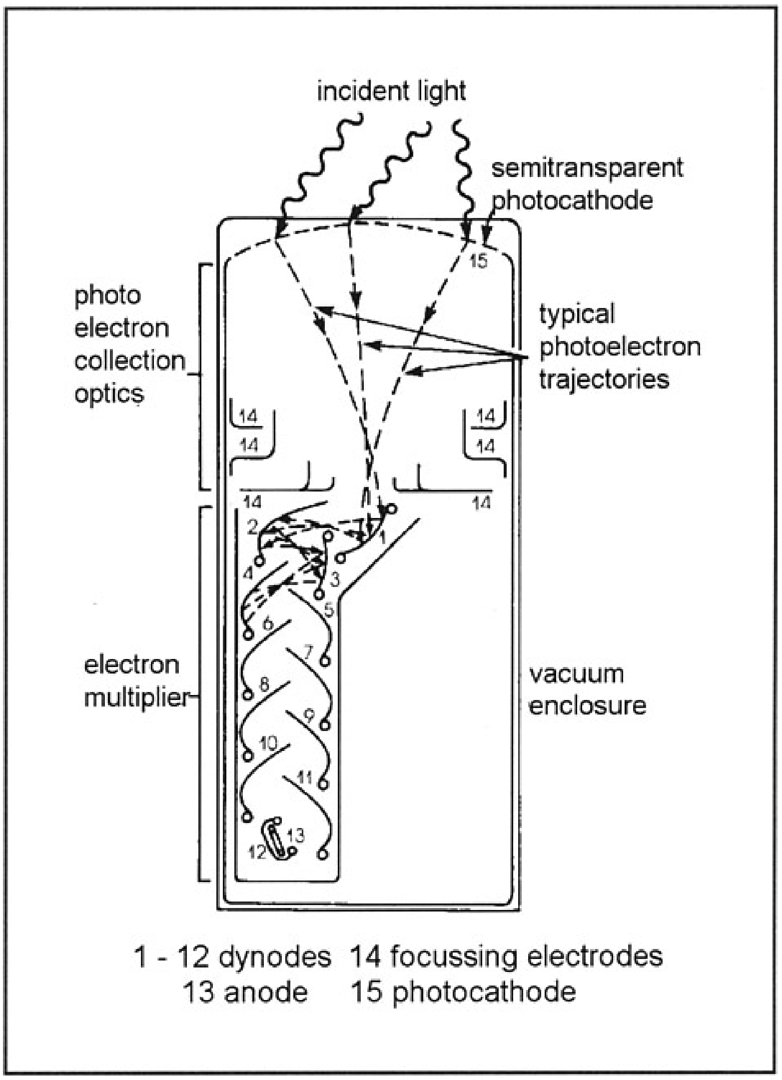

Figure 6: Schematic of a typical 12-stage Photomultiplier Tube[16].

3 Experimental Procedure

3.1 Verifying Emission Spectra

It is with this last aspect of the design of Super-NEMO that this project is concerned. It has been decided that polyvinyltoluene (PVT) scintillators will be investigated for use in Super-NEMO as they claim to have a higher light output than the polystyrene scintillator used by NEMO-III. The particular scintillators to be studied are BC-404, BC-408 and BC-412, manufactured by Bicron[8], and also a sample from Karkhov, who produced the scintillators for NEMO-III.

The wavelengths of maximum emission for the Bicron scintillator samples are stated as being 408 nm for BC-404, 425nm for BC-408, and 434nm for BC-412[4]. To ensure the most efficient combination of scintillator and PMT, these emission spectra must be independently measured and verified, using a commercially available spectrometer. Also the scintillator samples used will be of an appropriate geometry to approximate those for use within Super-NEMO, in $5 \times 5 \times 2$ cm^3 blocks.

An Ocean Optics USB2000 Miniature Fibreoptic Spectrometer was used, in conjunction with the OOIBase32 Spectrometer Operating Software. This allows real-time observation of the wavelength spectrum of light entering the spectrometer, which can then be saved either manually or automatically to a data file for later analysis. The USB2000 has an SMA connector (widely available) for the quick attachment of a fibre, which can be conveniently changed. Before any measurements could be taken using this device, it was necessary to gain a working knowledge of the spectrometer and associated software.

3.1.1 OOIBase32

OOIBase32 can be downloaded and installed from the Ocean Optics website, along with the operating manuals for both the software and the USB2000[17, 18]. These contain detailed instructions for the many features of the software, however for the purposes of this investigation only the Scope mode was used, with varying integration times. A wavelength spectrum as displayed by OOIBase32 can be seen in Figure 7, taken in scope mode with no fibre attached to the spectrometer. OOIBase32 does not seem to be a very stable program on modern systems, crashing regularly - when it is functioning correctly, however, it is quick and easy to take spectral data.

[8]The light outputs are (in % Anthracene) 68, 64 and 60 respectively[4].

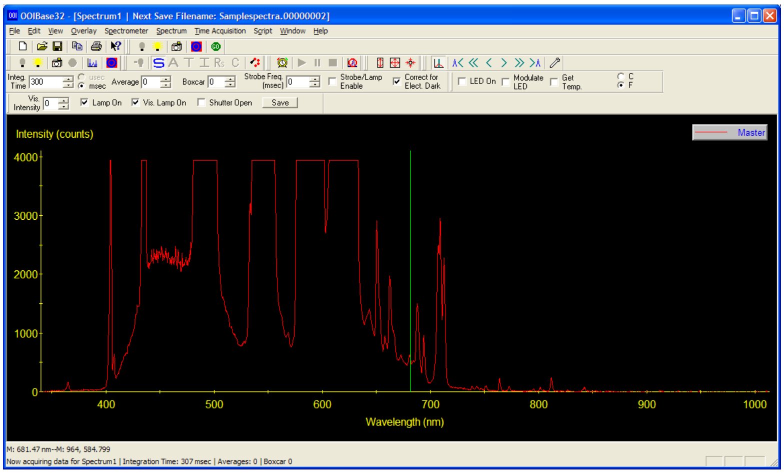

Figure 7: Screenshot of OOIBase32 in Scope mode, detecting ambient light, with an integration time of 300ms.

OOIBase32 only runs on Microsoft Windows releases up to 32-bit Windows XP, while the systems used for data analysis use CERN Scientific Linux and Mac OS X (both UNIX systems, meaning that the same data analysis software could be used on both). OOIBase32 saves a spectrum as both a `.Scope` and a `.Sample` file, which can only be read by OOIBase32 and other Ocean Optics software. When opened in a text editor these files were identical, and both contained header lines describing the parameters under which the data had been acquired. The file which produced Figure 7 is included in Appendix D[9]. As the integration time was the only thing varied within OOIBase32 it was decided that these lines could be deleted from the files prior to analysis. The platform and data format limitations of OOIBase32 meant that analysis of the spectra was not as straightforward as it could have been - while the transferring and editing of the data files was not challenging, it was time-consuming and did not allow for fast comparison between spectra.

3.1.2 Root

Root is a powerful Object-Oriented data analysis environment, developed at CERN, and freely available from the ROOT website[10], along with documentation and various tutorial exercises. It features a built-in `C++` interpreter, meaning that one can control it from the command line or from macros writ-

[9]This file is `Samplespectra.00000001.Master.Scope` and was subsequently edited to produce `roombackground1.dat`.

[10]`http://root.cern.ch/`

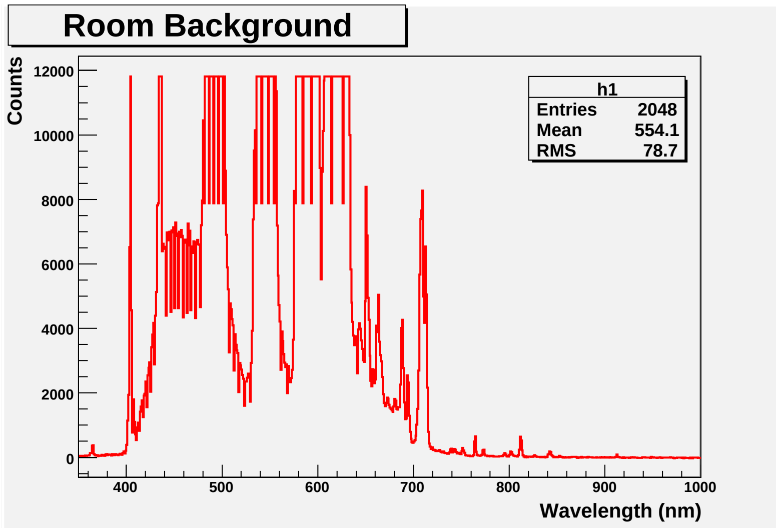

Figure 8: Histogram of ambient light in the Lab, produced using ROOT.

ten in C++. In order to produce histograms using ROOT, it was necessary to learn some C++ basics. The first working macro created was capable of reading in two columns of data from an ASCII file, and producing a histogram based on these data - this was `ledmacro2.cxx`[11], which required the ASCII file path to be edited for each histogram. This was used as a base for all other macros used in this investigation, and improved upon in many stages. Eventually macros were created that were capable of subtracting background readings from up to 5 collected spectra, the names of which are entered in the command line, normalising or scaling the integrals of their respective histograms and displaying them all on one plot with a legend. Various modifications to the appearance can then be made via the ROOT graphical interface or by saving the plot as a `.C` file and editing in a text editor - Figure 8 shows a histogram produced in ROOT using `roombackground1.dat` [12]

3.2 Finding the Energy Resolution

Once the emission spectra of the scintillators have been found, their energy resolutions can be compared using a radioactive source. ^{207}Bi was chosen for

[11]See Appendix E.1

[12]The maximum of the y-axis scale is three times that in Figure 7 (4000 counts) due to the binning of the data produced by OOIBase32 - the USB2000 collects data across 2048 pixels in the range 339.98 - 1013.98 nm, meaning that each bin in the histogram in Figure 7 is only 0.3nm. The bins in Figure 8 were set to 1nm to make the histogram easier to view.

this as it has two conversion electrons of energy 494 keV and 967 keV. The latter is very close to 1 MeV, where the target energy resolution of 7% lies. ^{207}Bi undergoes both β and γ decay, so in order to view the energy spectra of the electrons only it is necessary to remove the background photons from any data. The data was acquired using a CAMAC/NIM data aquisition system, consisting of a collection of ADC converters and logic gates - this is simply a way of connecting the PMT to a PC and collecting usable data. Energy data from the PMT used was taken for a chosen number (of the order of 10^5) of β and γ decays, then a 2mm thick sheet of aluminium can be placed between the source and the scintillator, as this will stop the electrons. The experiment can then be repeated for the same number of γ decays. This setup can be seen in Figure 9.

The two datasets are then normalised about the region where it is known that there are only γ decays, so that when the second dataset is subtracted from the first only the conversion electron energy spectrum remains. The 967 keV conversion electron peak is then fitted with a sum of three gaussians corresponding to the K, L and M lines of the 1064 keV transition[13]. This fit returns a σ_K and an E_K value, allowing the energy resolution at 967 keV to be calculated.

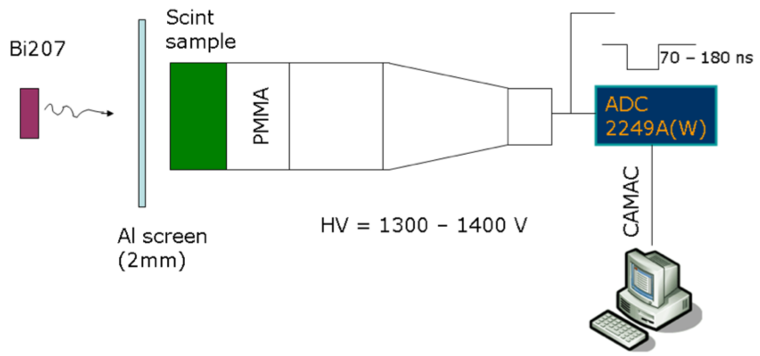

Figure 9: Schematic of the apparatus used to test the energy resolution of scintillator samples[2].

[13]The K, L and M lines correspond to 976 keV, 1049 keV and 1061 keV respectively.

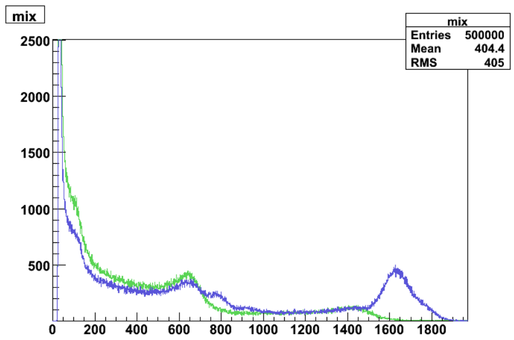

Figure 10: Energy spectra of both $\beta + \gamma$ and γ only, for ^{207}Bi.

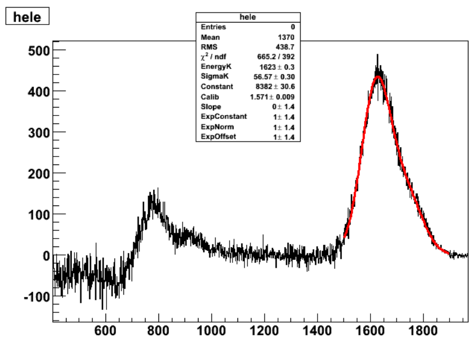

Figure 11: ^{207}Bi conversion electron spectrum obtained by subtracting γ from $\beta + \gamma$ (note the peaks at 482 keV and 976 keV).

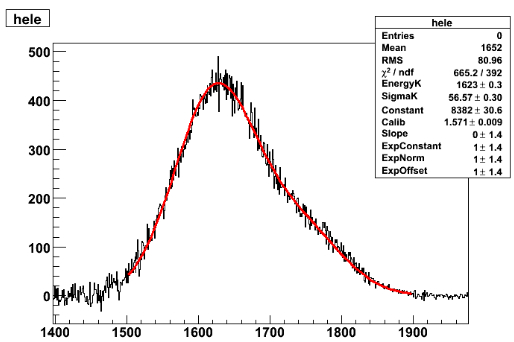

Figure 12: The 967 keV peak fitted with gaussians as described.

3.3 Data to be collected

Over the course of this investigation, the following data were to be collected:

- Wavelength spectra for LEDs with well-defined wavelengths, to establish accuracy and sensitivity of the spectrometer in the region of interest.
- Spectrum for a Mercury lamp, to compare measured spectral lines with those which should be produced, also for establishing the accuracy and precision of the spectrometer.
- Spectra for BC 408, BC-408, BC-412 and the Karkhov sample, stimulated using a Laser.
- Spectra for BC-408 in various positions, in order to see if different spectra are produced depending on the orientation of the Laser and the fibre.
- Spectra for the scintillators using an X-ray source, to establish whether the Laser can be used to simulate ionizing radiation.
- $\frac{\Delta E}{E}$ of the scintillators should be measured and compared with previous results.
- Quantum efficiency of the PMTs used should be combined with the emission spectra & light outputs of the scintillator samples, and used to estimate N_{pe} achievable for any particular PMT/scintillator combination.

4 Data Collection

This section contains material adapted from the author's Laboratory Notebook.

4.1 Preparation

Before being used to connect a scintillator to the spectrometer, the two ends of the fibre must be finely polished to ensure maximum light transmission. The fibre was inserted into an aluminium disc with a PTFE centre for stability and flexibility, and polished using RM Lapping paper of decreasing coarseness (50, 20, 12, 5 and 1 micron). The other end was glued into a 1mm diameter bore CONN-QSMA connector using Bicron BC600 optical cement[19], and when cured the connector was inserted into an aluminium disc (again, for stability) and polished using the same method. The polished fibre was then ready for gluing into the scintillator, or coupling to an LED[14].

4.2 151106

The first question to be addressed was the precision and accuracy that the spectrometer was capable of. A blue LED (LED0) was connected to the spectrometer using the polished fibre and BC625 optical gel, and also to an electrical signal generator. This allowed the pulse width, delay and voltage to be varied, while the spectra produced were saved for analysis. While taking these spectra it became apparent that OOIBase32 imposes a maximum limit of 4000 counts[15] for any particular wavelength - consequently, it was necessary to only vary the above quantities until this limit was reached, to avoid loss of information. These spectra could then be viewed and compared using ROOT.

4.3 221106

With the first data collected, the next task was to collect data from the scintillator samples. The first sample to be studied was a $5 \times 5 \times 2$ cm^3 block of BC-408. A 1.2mm diameter hole was drilled into one of the 5×2 cm^2 faces, into which the polished fibre was glued using BC600 optical cement as mentioned in 4.1. It was decided to use a 337nm laser to simulate incident radiation, meaning that when the scintillator was covered in Mylar a small gap was left through which the laser could be shone. The laser was capable of producing pulses from 1-20 Hz, however it was decided that in order to ensure continuity the frequency should always be set at the maximum.

For collection of data a simple adjustable system was created, which can be seen in Figure 13. This allowed the comparitive heights of the laser and scintillator to be easily adjusted, observing the displayed spectrum on the laptop to establish when the laser is lined up with the gap in the Mylar. This was necessary because a black cloth was placed over the entire apparatus to avoid ambient light entering the spectrometer, and also because it is not safe to directly view the laser light. Data was taken for two integration times, 2048 ms and 3072 ms. Multiple files were saved for each time (and also for all subsequent readings taken) in order to check the consistency of the spectra produced, and see if there was any significant change over time.

[14]The following sections are named by date in the same fashion as the directories (see Appendix B.2), as are all histograms produced throughout this report, allowing the precise data file(s) from which they are created to be easily identified.

[15]Throughout data collection, the integration time was mainly chosen as that which produced an emission peak as close to, but not more than, 4000 counts as possible.

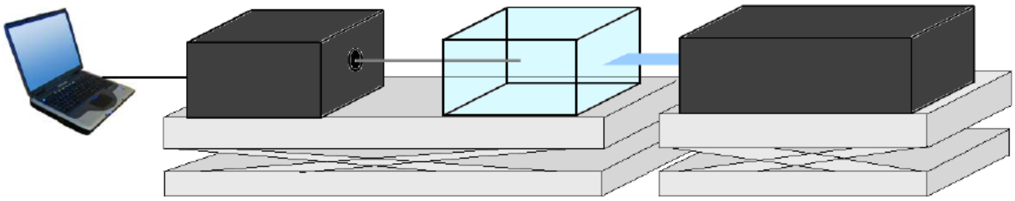

Figure 13: Schematic of scintillator setup, with components placed on scissor stands for adjustable height. From left to right: Laptop, *USB cable,* USB2000, *fibre,* scintillator (Mylar covering not shown), *laser beam,* laser.

4.4 190107

Using the same sample of BC-408, the orientation of the block with respect to the laser was changed - data was taken with the incoming laser beam parallel to the fibre (into the 5×2 cm^2 face) and perpendicular (into the 5×5 cm^2 face). Readings were taken with an integration time of 2048 ms. During this section of the experiment the fibre broke, causing the data to contain a large amount of background light and possibly also pure laser light.

The spectrum of the laser alone was also taken, by removing the scintillator and fibre shown in Figure 13 and adjusting the scissor stands (all covered in the black cloth) until the maximum reading was observed on the laptop. Many readings with varying integration times were taken.

4.5 260107

The emission spectrum of a mercury lamp was taken by attaching a polished fibre to the spectrometer and aligning it with the bulb of the lamp under the black cloth. 3 spectra were collected, all with integration time of 300 ms. Hg has very distinct emission lines, detailed in [3]. The matching of these with the observed spectra provided information about the accuracy of the USB2000. Emission spectra for another LED (LED 1) were also taken, at 300ms integration time. The LED was connected to the spectrometer as in section 4.2.

4.6 290107

The fibre broken in 4.4 was removed and replaced with a more robust one - the original Kuraray non-S type fibre was replaced with an ESKA fibre which should withstand more manipulation. This fibre was glued back into the same block of BC-408, as described in 4.3 except that the hole was drilled into the 5×5 cm^2 face, for further investigation into the effects of the orientation of the fibre on the emission spectrum. Spectra were taken at 1024 ms and 2048 ms. Also spectra for a "UV LED" (LED2) were taken, all with an integration time of 300 ms.

4.7 080207

The next sample to be studied was BC-404. The hole was drilled into the 5×2 cm^2 face and a polished ESKA fibre was glued in place. The integration times used were 2048 ms and 3072 ms.

4.8 140207

Energy resolution data for BC-404 and BC-408 was taken during the process of learning to operate the equipment (described in section 3.2), over 5×10^5 events.

4.9 210207

An X-ray set was used to take spectra of BC-404 - the X-ray source was a copper tube with a tungsten filter, operating at 40 keV and 25 mA. Part of the apparatus in Figure 13 was used, placing the left scissor stand within the case of the X-ray set, and directing the beam onto the scintillator. A lead screen was placed between the spectrometer and the laptop (which was outside the X-ray case) for safety. While taking the first 5 readings (integration time of 3072 ms), it was noticed that there was a large amount of background radiation interfering with the observed spectrum, so two background readings were taken with the X-ray set switched off and an integration time of 9216 ms, to be subtracted from the measured scintillator spectra. Ten spectra were then taken with the X-ray set on, also with an integration time of 9216 ms.

4.10 230207

The BC-412 sample was drilled and glued as before, and using the laser 5 readings were taken with an integration time of 5120 ms. Background readings were taken as well, to identify the levels of ambient light under the black cloth.

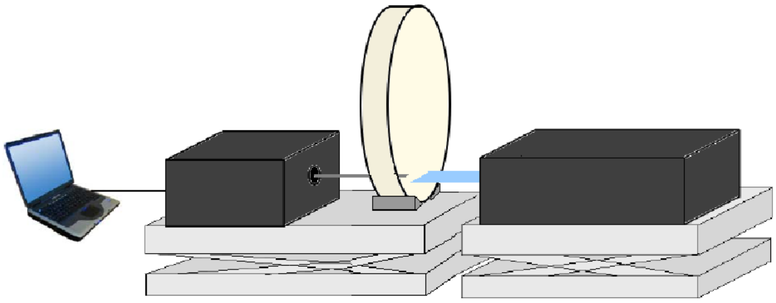

Figure 14: Schematic of scintillator setup as modified for the Karkhov sample, held in place with small metal wedges.

4.11 270207

The sample of polystyrene scintillator, the Karkhov sample, is not a $5 \times 5 \times 2$ cm^3 block like the Bicron scintillators - it is a 12 cm diameter disk, 2 cm thick, with an opaque white coating on all but one side. A hole was drilled into the covered circular side, allowing the sample to be positioned much as the Bicron samples were, shown in Figure 14. 10 readings were taken with 1024 ms, as well as three background readings with the laser turned off and the black cloth still in place.

4.12 280207

The same X-ray set was used as in section 4.9, and background and emission spectra for both BC-412 and the Karkhov sample were taken, all with an integration time of 9216 ms.

4.13 070307

Energy Resolution data was taken for BC-412 over 5×10^5 events. This was then repeated the following day, due to anomalies in the data.

5 Results

5.1 Sensitivity of the Spectrometer

The LEDs studied, referred to above as LED0, LED1 and LED2, were found to have spectral means of 470nm, 475nm and 403.5nm respectively. Multiple readings were taken for each LED, some of which can be seen in Figure 15. Figures 15a and 15b show the spectra taken for LED0 both before and after normalising their integrals to 1. The similarity of these 5 histograms suggest that the spectrometer is unaffected by changes in amplitude and frequency of incoming light. The spectra for LED1 and LED2 show that the spectrometer is capable of producing consistent results at various wavelengths. In Figure 15c the histograms are so similar that they are almost indistinguishable from one another - the maximum difference between two readings at the peak wavelength is less than 0.6% (looking in detail at the peak of the histogram).

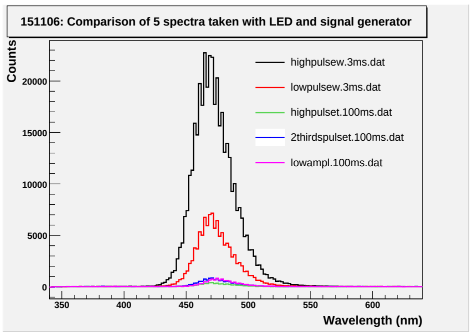

(a) 5 Unscaled Spectra for LED0 under different conditions.

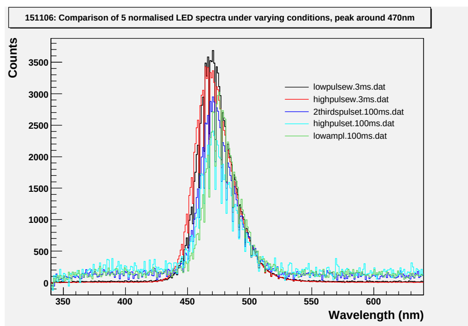

(b) 5 Spectra for LED0 scaled to have equal integrals.

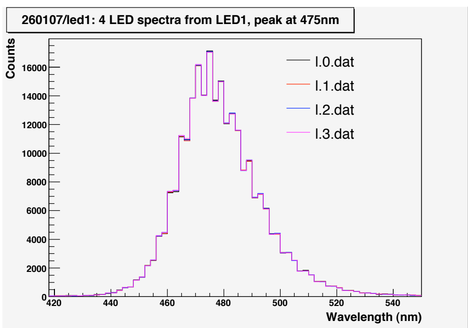

(c) 4 spectra for LED1.

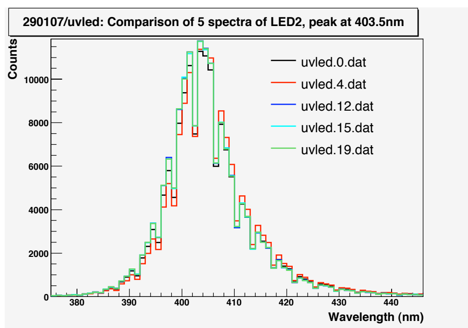

(d) 5 spectra for LED2.

Figure 15: LED spectra.

Measured λ (nm)	Nearest listed λ (nm)
364-366	365.0
	365.5
	366.3
403-406	404.7
407-409	407.8
434-437	434.8
	435.8
542-548	546.1
577-582	577.0
	579.1

Table 1: Comparison of observed Hg spectral lines with values from [3].

Now that the sensitivity of the spectrometer has been established, the accuracy must be checked. For this the Hg lamp spectrum is used, and the spectral lines observed[16] are compared with a table of values, as shown in Table 1. It can be seen that the measured spectrum corresponds very well with the expected readings, as all spectral lines are observed at the expected wavelengths. From this the spectrometer can be said to be accurate down to a range of about 10^{-9}m, which is ample for the purposes of this investigation.

5.2 Emission spectra of the Scintillators

5.2.1 Laser

Figure 16 shows the emission spectra for the four scintillator samples, using the Laser to produce scintillations. As with the LEDs, 5 spectra have been displayed on the same plot to demonstrate the consistency of results. These histograms have not been scaled or normalised in any way. Figures 16c and 16d also contain the background light reading (in pink). As can be seen, this is negligible compared to the spectra themselves.

Figure 17 shows the emission spectra of all four scintillators on the same plot, all normalised to have equal integrals[17].

[16]Figure 23 in Appendix C.

[17]It should briefly be noted that the variations in orientation of scintillator and optical fibre investigated in sections 4.4 and 4.6 showed no significant variation in the acquired spectra, once the problem of the broken fibre had been identified. This can be seen in Figure 25 in Appendix C.

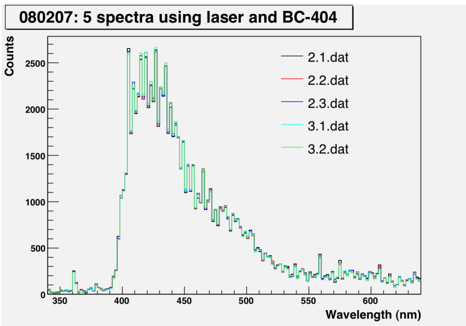

(a) 5 Laser spectra for BC-404.

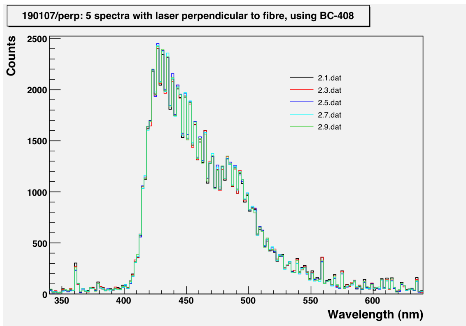

(b) 5 Laser spectra for BC-408.

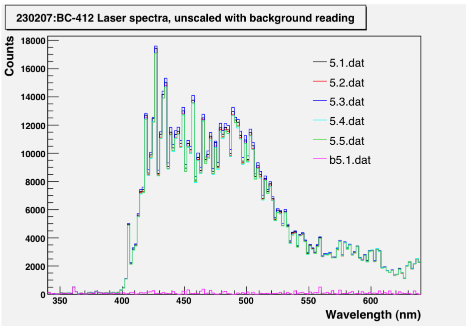

(c) 5 Laser spectra for BC-412, with background.

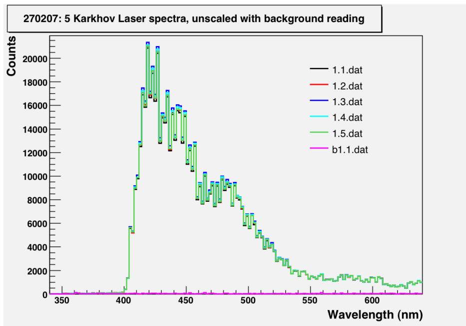

(d) 5 Laser spectra for the Karkhov sample, with background.

Figure 16: Laser Spectra

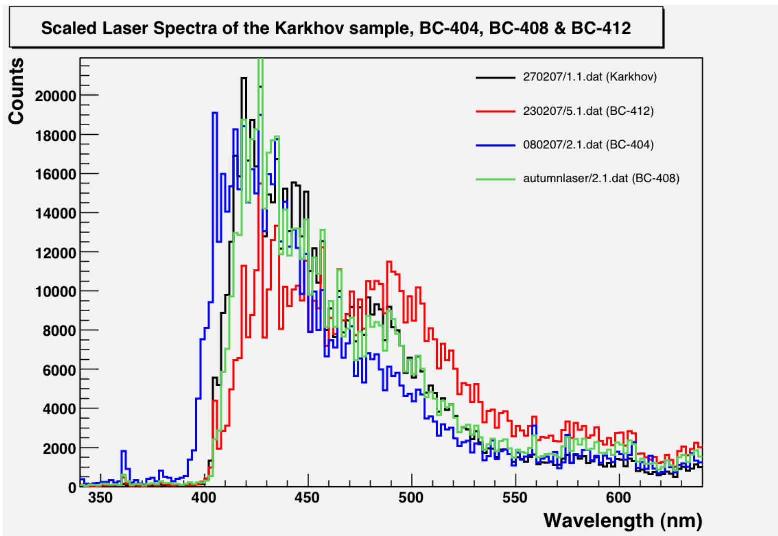

Figure 17: Normalised Laser spectra for all four scintillators.

5.2.2 X-ray

The spectra obtained using the X-ray set had a significant amount of background noise, partly because it was not possible to block out all light while taking readings. Consequently, for each sample tested a background light reading with the same integration time was also taken. When this reading was subtracted from the scintillator spectra, a pure spectrum was produced for comparison with the Laser spectra - histograms showing these spectra can be seen in Figures 26-28 in Appendix C. The extra shoulders, especially in BC-412, could possibly have been attributed to some unknown mechanism within the scintillator when using the Laser, however this does not seem to be the case as the same shoulders occur when using X-rays. Further analysis of the shape of the X-ray spectra can be found in Appendix A.1. The X-ray and Laser spectra are compared in Figure 18, and it can be seen that the positions of the wavelengths of peak emission coincide well in the region up to 550nm. Based upon this, it was decided that the Laser could be used to approximate the ionizing radiation of X-ray or β decays. The tail above 550nm can be neglected, as will be discussed in section 5.4.

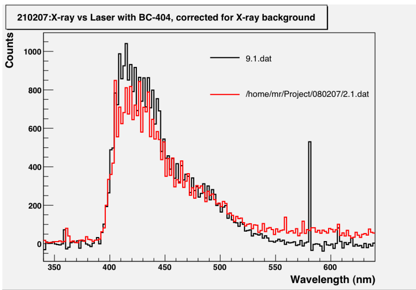

(a) Laser and X-ray spectra for BC-404.

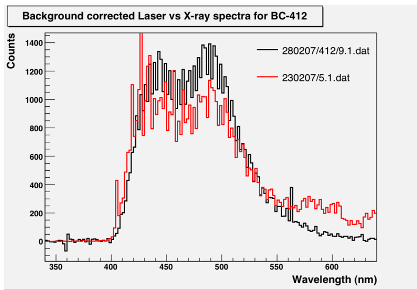

(b) Laser and X-ray spectra for BC-412.

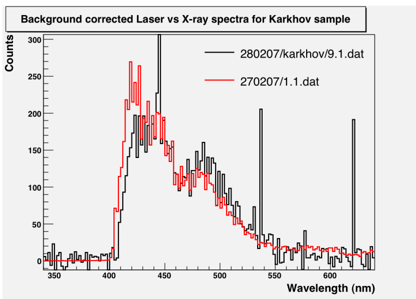

(c) Laser and X-ray spectra for the Karkhov sample.

Figure 18: Comparison of X-ray and Laser Spectra

5.2.3 Comparison with Manufacturer's Data

Reference [4] contains emission spectra for BC-404, BC-408 and BC-412. These spectra[18] can be seen in Figure 19a. These spectra can now be compared with the measured Laser spectra; the measured spectra in Figure 19b were rebinned and renormalised to allow visual comparison. The peak positions are clearly not the same - Table 2 compares the values given by Bicron with those gained by inspection of Figures 17 and 20. The spectra appear to have become stretched towards longer wavelengths, shifting the positions of the shoulder areas and increasing their amplitude relative to the peak. This spreading may possibly be attributed to the geometry of the scintillator blocks, as the dimensions of the scintillators tested to produce the Bicron spectra are not known.

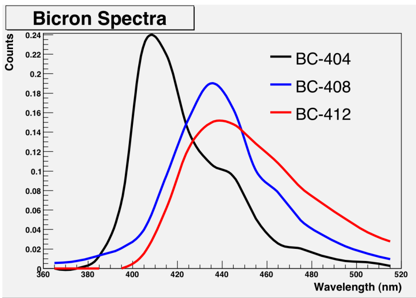

(a) Emission Spectra created from data provided by Bicron.

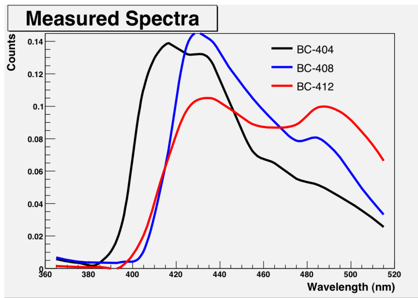

(b) Emission Spectra as measured.

Figure 19: Comparison of measured Spectra with those provided for the Bicron Scintillators.

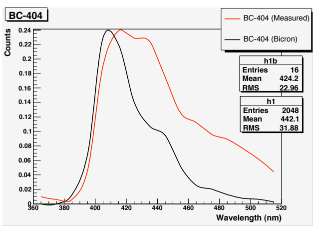

(a) BC-404

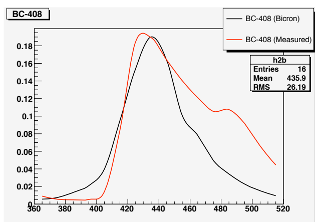

(b) BC-408

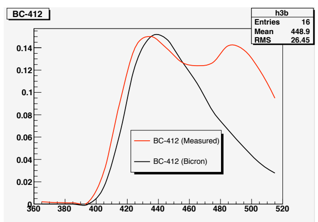

(c) BC-412

Figure 20: Individual comparisons of measured and Bicron Spectra.

---

[18] Adapted from those shown in Figure 29 in Appendix C.

Scintillator	Bicron λ_{max} (nm)	Measured λ_{max} (nm)
BC-404	408	417±3
BC-408	425	427±1
BC-412	434	434±2
Karkhov	n/a	418-425

Table 2: Comparison of observed Wavelengths of Maximum Emission (λ_{max}) with values from [4].

5.3 Finding the Energy Resolution

As the Karkhov sample was not available in a $5 \times 5 \times 2$ cm^3 block, it was only possible to obtain energy resolutions for the Bicron scintillators. These are shown in Table 3, although these are not very accurate values as they are each based on the first and only datasets taken, due to time restraints. These values can be compared to those listed in [2] when using a Mylar covering and a 5” ETL PMT. Figures 30 and 31 in Appendix C show the fits from which the energy resolutions of BC-408 and BC-412 are calculated.

Scintillator	Size, cm^3	Coating	R6233 $\frac{\Delta E}{E}$, (%)	ETL $\frac{\Delta E}{E}$, (%)
BC-404	$5 \times 5 \times 2$	Mylar	7.8	7.8
BC-408	$5 \times 5 \times 2$	Mylar	8.2	8.2
BC-412	$5 \times 5 \times 2$	Mylar	10.4	n/a

Table 3: FWHM Energy resolution for 967 keV electrons using the R6233 PMT compared to that for 1 MeV electrons obtained with the 5” ETL phototube[2].

5.4 Effects of Quantum Efficiency on Emission Spectra.

The PMT used to find the energy resolution was a Hamamatsu R6233MOD High Q.E. Photomultiplier Tube. The manufacturers provided information about the Q.E. of this PMT, both in graphical and digitized form (See Figure 32 in Appendix C). Multiplying the emission spectra by their light output and then by the Q.E. should give histograms with integrals proportional to N_{pe}, which can then be used to give an approximation of the energy resolution obtainable according to the manufacturers data.

For the emission spectra, the square root of ratio of their integrals, I, should be inversely proportional to the ratio of their energy resolutions as shown in Equation 11. From Table 4 it can be seen that the ratio of energy resolutions for BC-404 : BC-408 : BC-412 should be 1 : 1.05 : 1.11, however it is measured as 1 : 1.05 : 1.27. By inspection of Figure 19 a reason for this imbalance can be proposed. BC-412 appears to have a secondary peak, or shoulder, around 490 nm, at which point the Quantum Efficiency of the PMT is falling below 25%. This means that little of the light at or above this wavelength is converted into photoelectrons, reducing the integral of the histogram and worsening the energy resolution (This can be seen in Figure 33 in Appendix C). This also goes to explain why the tail above 550 nm can be neglected (see section 5.2.2), as at these wavelengths the Q.E. is below 10%.

These ratios can be checked using the measured emission spectra. When normalised and multiplied by the Q.E. distribution, the ratios of the integrals can be compared and used to find the energy resolution. Figure 22 shows the measured emission spectra before and after convolution with the Q.E. of the PMT[19]. By this method it is possible to estimate a value for the energy resolution of a scintillator with a certain PMT purely by knowing the emission spectrum and Q.E. distribution, providing one has obtained an energy resolution for at least one other scintillator. Table 5 shows the integrals and gives an estimate for the energy resolution of the Karkhov sample. From the ratios of the integrals of BC-404, BC-408 and BC-412 the energy resolution of the Karkhov sample is estimated to be 9.4%, 9.0% and 9.9% respectively.

$$\frac{\Delta E/E(a)}{\Delta E/E(b)} = \frac{\sqrt{N_{pe}(b)}}{\sqrt{N_{pe}(a)}} \tag{11}$$

Scintillator	$I\times$ Q.E.	a:b	$\sqrt{N_{pe}(a)}/\sqrt{N_{pe}(b)}$	$\frac{\Delta E}{E}$(b)/$\frac{\Delta E}{E}$(a)
BC-404	22	404:408	1.05	0.95
BC-408	20	408:412	1.05	0.95
BC-412	18	404:412	1.11	0.91

Table 4: Integrals and ratios of the histograms in Figure 21, with predicted $\frac{\Delta E}{E}$ ratios.

[19]The light output of the Karkhov sample has been conservatively estimated as 55% Anthracene - the wavelength of peak emission was observed at between 418 and 425 nm. From [20] it was discovered that the scintillators made by Karkhov which had peaks in this region all had a light output of 55-60%.

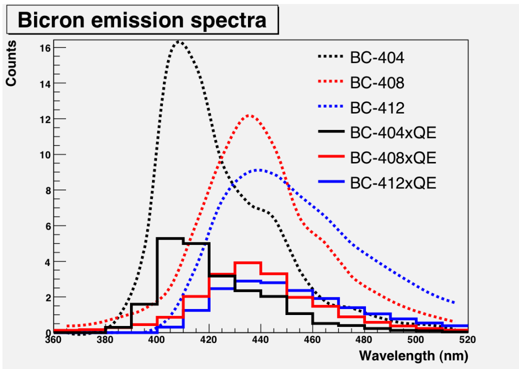

Figure 21: Manufacturers' emission spectra multiplied by the Q.E. of the R6233 PMT.

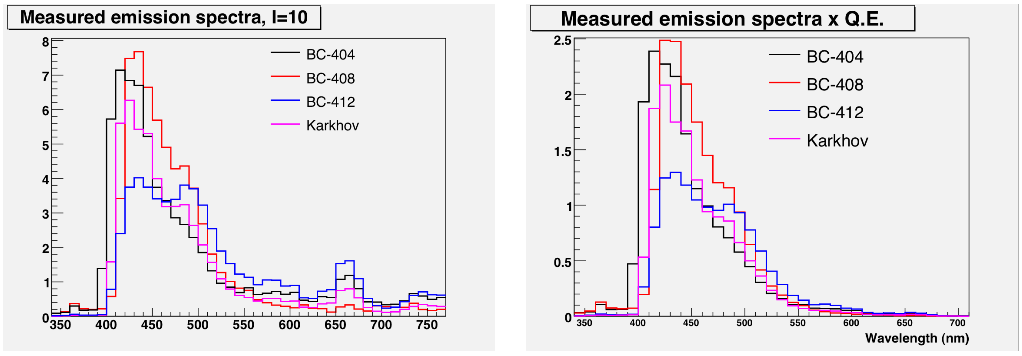

(a) Integral = Light Output

(b) Multiplied by R6233 Q.E.

Figure 22: Measured emission spectra for all four scintillator samples, normalised to the light output and then multiplied by the Q.E. of the R6233 PMT.

Scintillator	$I\times$ Q.E.		Scintillator	$I\times$ Q.E.
BC-404	17.183		BC-408	17.283
BC-412	12.819		Karkhov	14.261
Scintillators (a:b)	$\frac{\sqrt{N_{pe}(a)}}{\sqrt{N_{pe}(b)}}$	$\frac{\Delta E}{E}(\mathrm{b})/\frac{\Delta E}{E}(\mathrm{a})$		
		Predicted	Measured	% difference
404:408	1.00	1.00	0.95	5.3
408:412	1.16	0.86	0.79	8.9
404:412	1.16	0.86	0.75	14.6
404:Karkhov	1.10	0.83	-	-
408:Karkhov	1.10	0.91	-	-
412:Karkhov	0.95	1.05	-	-

Table 5: Integrals and ratios of the histograms in Figure 22.

6 Conclusions

The initial aims of this investigation were to find the emission spectra for the four scintillator samples and compare them with the spectra provided by the manufacturer, Bicron. As can be seen above, the spectra differ greatly, meaning that any PMT choice based on the Bicron spectra could have excluded a large proportion of the photons produced by the scintillators, and resulted in a less than optimum energy resolution. The unexpected shape of the spectra cannot be dismissed as being down to the method of producing scintillations, as the effects are present on both Laser and X-ray spectra.

The measured spectra can now be used in simulations of Super-NEMO events; the number of photons produced per MeV is intrinsically related to $\frac{\Delta E}{E}$ and so using the measured spectra will certainly affect the energy resolution of the calorimeter in simulations of $\beta\beta$ events.

The shape of the spectra seems likely to be due to the geometry of the sample. The standard method of measuring the emission spectra of scintillators is by shining a laser onto the surface of the scintillator and measuring the reflected light, which is equivalent to directly measuring the emission spectrum of a very thin sample of scintillator. This does not allow for repeated absorption and reemission at longer wavelengths, as seems to be occuring in the 2 cm thick samples studied - this would account for both the apparent "stretching" of the spectra and also for the change in relative prominence of the primary and secondary (shoulder) peaks in the spectra - as the shift occurs, more light is likely to be observed at the shoulder compared to the unshifted spectra. This is, however, only one reason proposed, and further research is necessary to reach a conclusion.

The energy resolutions previously obtained for BC-404 and BC-408 have been accurately reproduced experimentally using a different PMT, as shown in Table 3. The energy resolutions obtained for the Bicron scintillators are promising - improvements are definitely possible by varying the covering of the scintillator from Mylar, and also use of a green-extended PMT could dramatically improve the energy resolution. It should be noted that none of the scintillator samples emit any light below 395 nm and very little is emitted above 550 nm, so the Q.E. of the chosen PMT outside this wavelength range is irrelevant. The Hamamatsu R6233 PMT has highest Q.E. from 300 - 500 nm, with a peak of 34.9% at 350 nm. If a green-extended PMT with a similar distribution and a peak Q.E. at around 430 nm could be found[20],

[20]If this same Q.E. spectrum could be shifted to longer wavelengths by approximately 100 nm the effect on the energy resolution achievable would be large, improving $\frac{\Delta E}{E}$ for BC-404, BC-408 and BC-412 to 7.3%, 7.6% and 9.0% respectively - these numbers are obtained from the ratios of the integrals in Figure 34 in Appendix C.

the improvements to the energy resolutions would be significant. It is also possible to change the chemistry of the scintillators, shifting the emission spectra towards shorter wavelengths and maximising N_{pe} this way instead. Certainly an energy resolution of 7% at 1 MeV seems within reach.

It has also been possible to use emission spectra and the Quantum Efficiency of a particular PMT to make an estimate of the achievable energy resolution for the Karkhov sample, as well as making an estimate of the light output based upon the wavelength of maximum emission. This method could be used to approximate the energy resolution of a scintillator sample before detailed investigation were to take place, as a way of screening out unsuitable samples. This method could also be used as a rough "sanity check" for measured energy resolutions.

As a result of the findings of this project the need to study some further aspects of calorimeter design has come to light, as outlined in Appendix A.

References

[1] A S Barabash (on behalf of the Nemo collaboration). Nemo-3 and supernemo double beta decay experiments. *Journal of Physics: Conference Series*, 39:347–349, 2006.

[2] R.Saakyan, J.Thomas, S.Söldner-Rembold, and A. Pilaftsis. Proposal for the super-nemo design study, 2005.

[3] C. J. Sansonetti, M. L. Salit, and J. Reader. Wavelengths of spectral lines in mercury pencil lamps. *Applied Optics*, 35:74–77, January 1996.

[4] Saint-Gobain Ceramics & Plastics Inc. *Premium Plastic Scintillators Data Sheet*, 2005.

[5] K2K Collaboration: M. H. Ahn. Measurement of neutrino oscillation by the k2k experiment. *Physical Review D*, 74:072003, 2006, arXiv:hep-ex/0606032.

[6] H. V. Klapdor-Kleingrothaus, A. Dietz, H. L. Harney, and I. V. Krivosheina. Evidence for neutrinoless double beta decay. *MOD.PHYS.LETT.A*, 16:2409, 2001, arXiv:hep-ph/0201231.

[7] NEMO Collaboration: François Mauger. Physics goals - the double beta decay. Webpage: `http://nemo.in2p3.fr/physics/dbd.php`, 2004.

[8] Werner Rodejohann. Neutrinoless double beta decay and the neutrino mass matrix. *Physica Scripta*, 2006(T127):35–37, 2006.

[9] C. E. Aalseth et al. Comment on "evidence for neutrinoless double beta decay". *MOD.PHYS.LETT.A*, 17:1475, 2002.

[10] R. Arnold et al. First results of the search for neutrinoless double-beta decay with the nemo 3 detector. *Physical Review Letters*, 95(18):182302, 2005.

[11] Nuclear University of Zaragoza and High Energy Physics Laboratory. Webpage: `http://www.unizar.es/lfnae/grafs/2beta.gif`, 2004.

[12] M. Nomachi et al. Moon (mo observatory of neutrinos) for double beta decay. *Nuclear Physics B - Proceedings Supplements - Proceedings of the Eighth International Workshop on Topics in Astroparticle and Underground Physics*, 138:221–223, January 2005.

[13] Dominique Lalanne. Anti-radon facility at fréjus laboratory for nemo 3. Presentation, 2004.

[14] Richard B. Firestone and Virginia S. Shirley, editors. *Table of Isotopes*. John Wiley & Sons, Inc, 8 edition, 1998.

[15] R. Saakyan. Supernemo $0\nu\beta\beta$ experiment - present status and future plans. Presentation, October 2006.

[16] SCIONIX Scintillation Detectors. *Scintillation Detectors Overview*.

[17] Ocean Optics B.V. (Europe), Geograaf 24, 6921 EW DUIVEN, The Netherlands. *OOIBase32 Spectrometer Operating Software - Installation and Operation Manual*.

[18] Ocean Optics B.V. (Europe), Geograaf 24, 6921 EW DUIVEN, The Netherlands. *USB2000 Fiber Optic Spectrometer - Installation and Operation Manual*.

[19] B. Anderson. Glues etc. Pers. Comm., February 2007.

[20] Amcrys-H Scintillator materials and detectors, Karkhov, Ukraine. *Physical Properties of Plastic Scintillators*, 1998.

[21] Helen Moyses via R.Saakyan. Spectral response characteristics of tube type : R6233-100. Pers. Comm., February 2007.

[22] Rene Brun and Fons Rademakers. *ROOT Tutorials*, May 2001.

Appendices

A For Further Investigation

A.1 Shape of X-ray and Laser Spectra

The X-ray and Laser spectra, while broadly matching, do not display the same characteristics. Although the differences do not have any bearing within the scope of this investigation, it is of interest to examine the differences more closely. The top of the spectra exhibit unexpected fluctuations which were at first thought to be due to the method of data aquisition. With a bin width of 6 nm this effect seems to be removed, however with a bin width of 4 nm the effect is reduced in the X-ray spectra but remains in the Laser spectra. The rebinned spectra are shown in Figures 35a to 37a with the effect still visible, and reduced in Figures 35b to 37b. This shape could be due to the higher light intensities observed in the Laser spectra producing unexpected effects within the scintillator, or possibly the spectrometer introduces errors at high intensities.

A.2 Light Outputs

The light outputs referred to throughout this report have been those given by the scintillator manufacturers, and have yet to be verified. Under controlled, low background conditions it should be possible to use the same methods used to take emission spectra to take light output data. If the integration times used for all four scintillators were identical, it should be possible to obtain at least relative light outputs from the spectra produced, by comparing their integrals between certain wavelengths.

A.3 Transmission Spectra

The transmission spectra of the scintillators should be obtainable by dividing the Bicron spectra by the measured spectra. However, as the positions of the peaks in the spectra do not correspond, this has not been possible. In theory, if the measured spectra were to be normalised so that the content of each bin was never more than the content of the corresponding bin in the Bicron spectra, it should be possible to obtain the transmission spectra. In practice however this does not seem to produce useful results, as shown in Figure 24 in Appendix C. OOIBase32 has a Transmission mode, which there was not enough time to investigate, but which may prove useful for directly measuring the transmission spectra of the scintillators, and comparing them to those obtained as mentioned above.

B Notes

B.1 Personal Development

This project required extensive use of ROOT requiring me to become familiar with both ROOT and the `C++` programming language. Also I became proficient at using the Linux operating system, and at using LaTeX with which this report was written - specifically using PDFTeX and BibTeX under Aquamacs Emacs. This allowed me to help others who were also writing their reports, and I feel that the skills aquired during this investigation will stand me in good stead in the future.

While I had used ROOT a little before, I had not fully grasped the flexibility of using macros to produce histograms. A few of the 40+ macros I wrote are included in Appendix E - these are the final working versions, and also the ones I used most. Also, large parts of the code included here were used as a base for most of the other macros created during the course of this project.

All of the figures in this report, their accompanying macros and data files, the `.tex` files used to produce this report and all other work submitted as part of this project can be found at `http://www.hep.ucl.ac.uk/~mr/`.

B.2 Directory Structure

When collecting data, the files produced were saved in the following directory structure: `~/Project/[ddmmyy]/t.n.dat`, where `t` is the integration time in seconds or ms and `n` runs from from 1 to the number of spectra saved with that particular `t`. This makes it simple to keep track of which readings pertain to which results, and also permits faster filename input to the macros as the names automatically generated by OOIBase32 are very long. Each date-labelled directory also contains a file `details.txt` which explains the naming of the files.

C Histograms

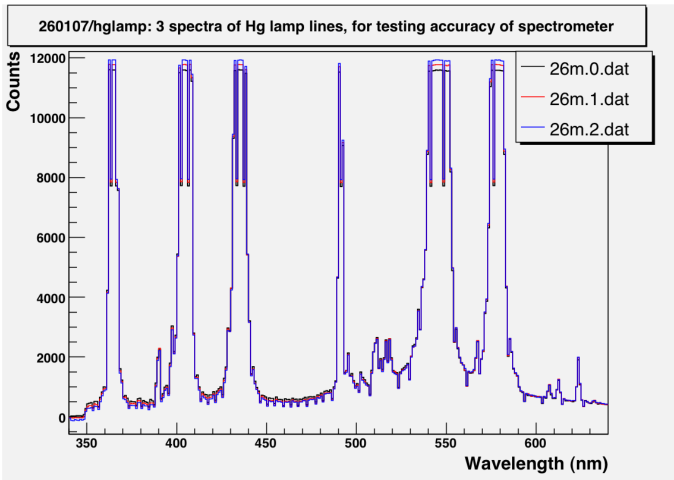

Figure 23: Mercury Lamp Spectra.

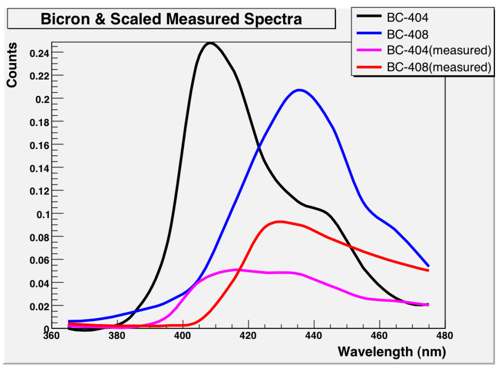

(a) Expected and measured spectra.

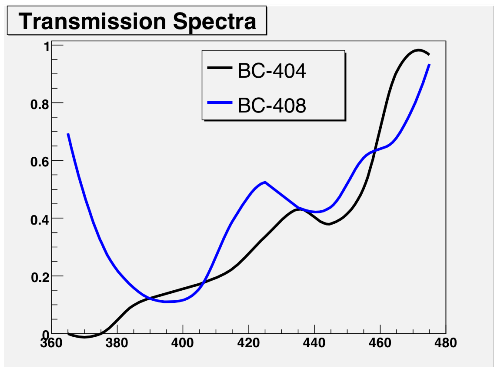

(b) Transmission spectra (Measured/Expected spectra).

Figure 24: Transmission spectra of BC-404 and BC-408

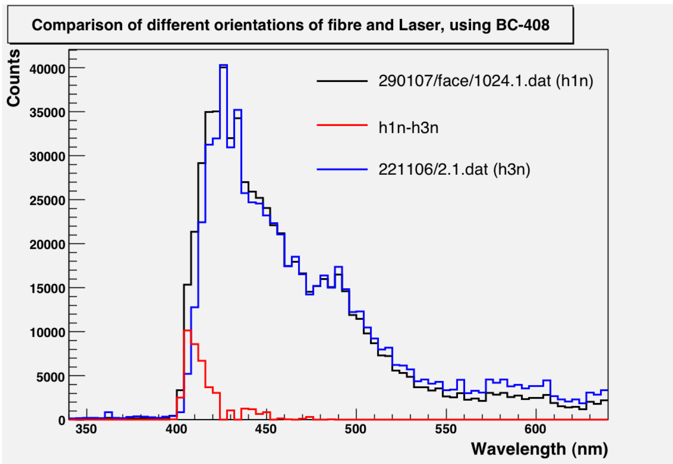

Figure 25: Histograms of the spectra taken with BC-408 with the fibre glued into the 5 × 5 cm face and the 5 × 2cm face, and the difference between the two.

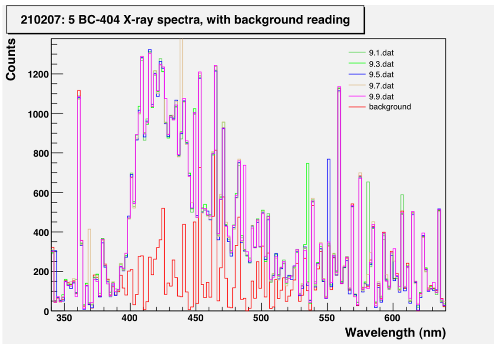

(a) 5 raw X-ray spectra for BC-404.

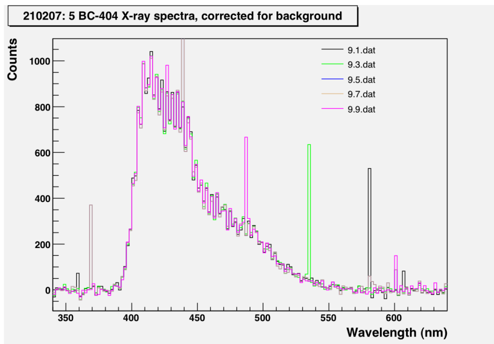

(b) 5 X-ray spectra for BC-404 (background subtracted).

Figure 26: BC-404.

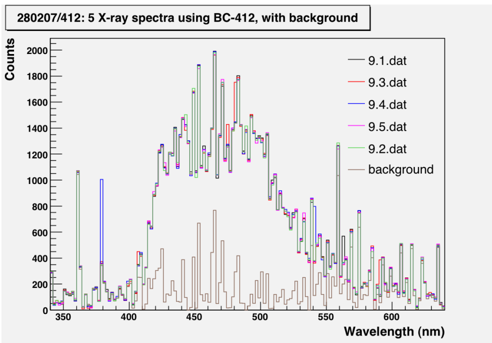

(a) 5 raw X-ray spectra.

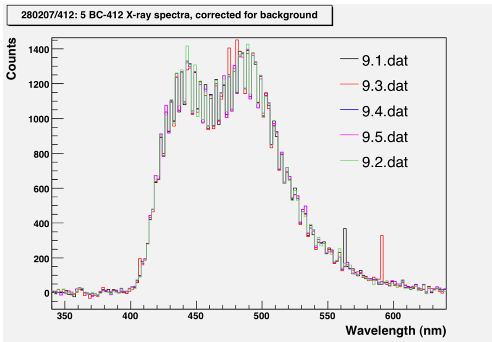

(b) 5 X-ray spectra (background subtracted).

Figure 27: BC-412.

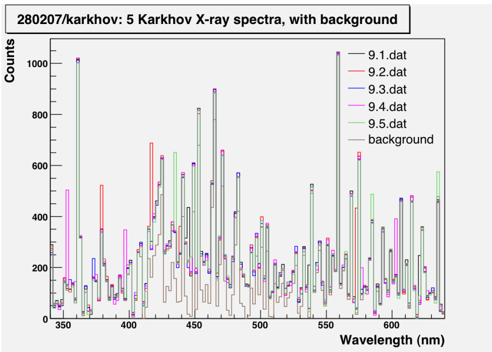

(a) 5 raw X-ray spectra for the Karkhov sample.

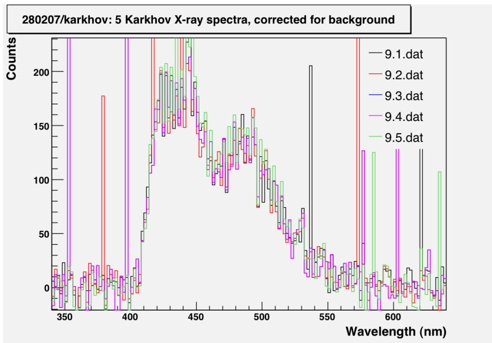

(b) 5 X-ray spectra for the Karkhov sample (background subtracted).

Figure 28: Karkhov.

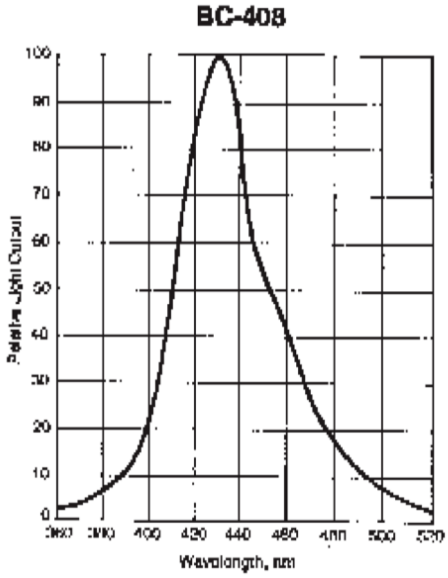

(a) BC-408

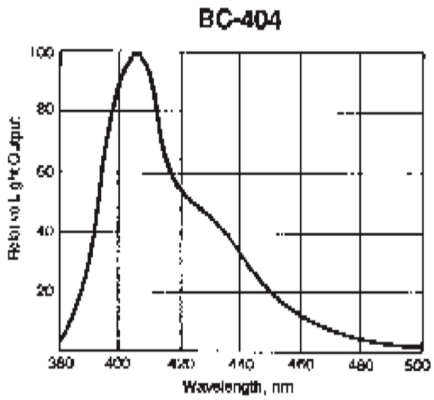

(b) BC-404

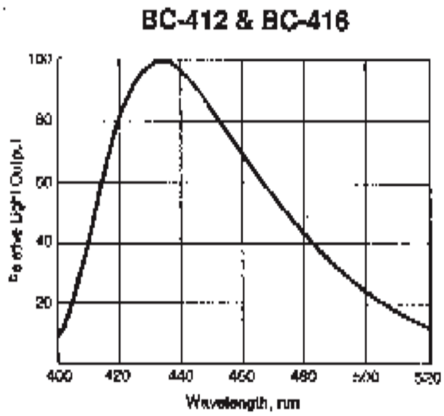

(c) BC-412

Figure 29: Emission spectra of the Bicron scintillators, as provided by the manufacturer[4]. The values at 10nm intervals were read from these figures and used to produce histograms in ROOT for comparison with measured spectra.

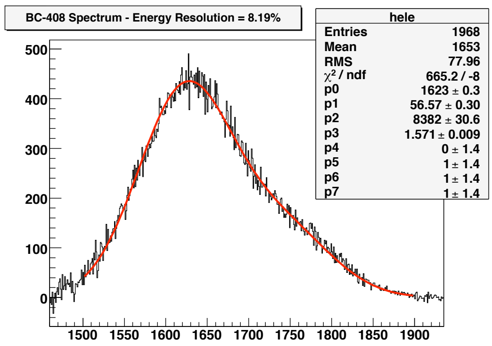

Figure 30: Energy resolution fit for BC-408, with 500000 events.

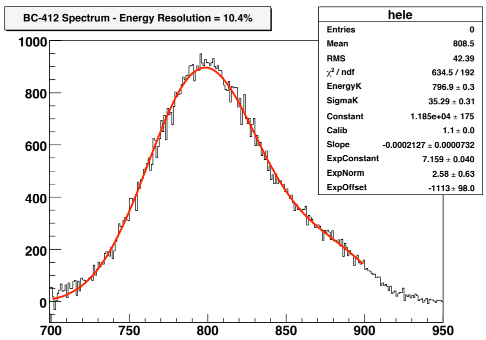

Figure 31: Energy resolution fit for BC-412, with 500000 events.

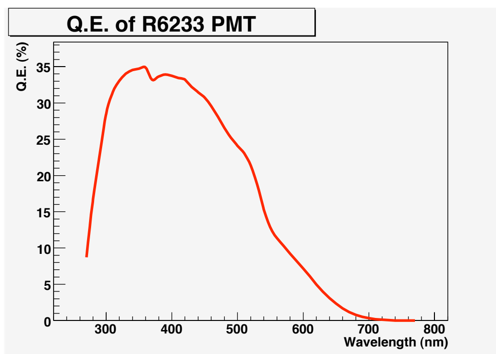

Figure 32: Quantum Efficiency of R6233 PMT[21].

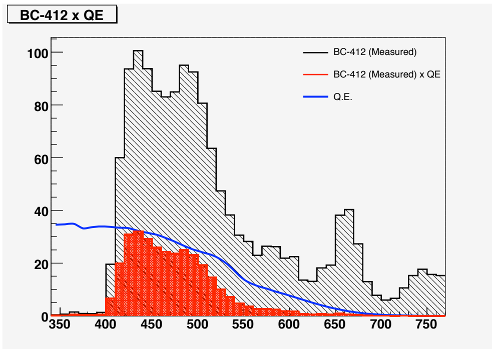

Figure 33: BC-412 spectra before and after multiplying by the Q.E. (also shown) of the R6233.

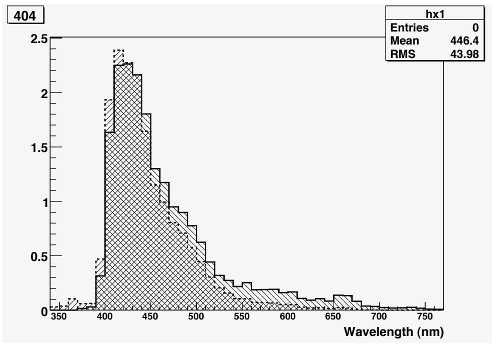

(a) BC-404.

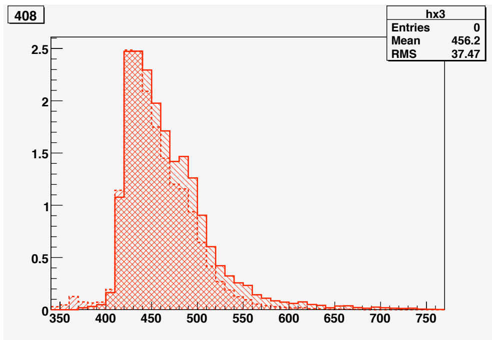

(b) BC-408.

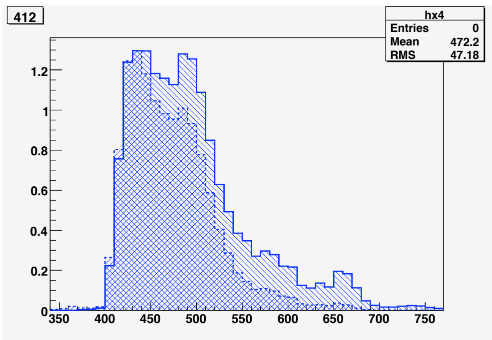

(c) BC-412.

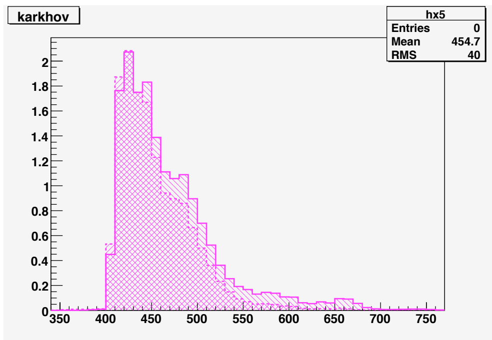

(d) Karkhov.

Figure 34: Postulated spectra with a green-extended PMT - dotted line is with R6233, solid line is with the Q.E. spectrum shifted by 100 nm towards longer wavelengths. The lightly shaded area is the improvement in N_{pe}.

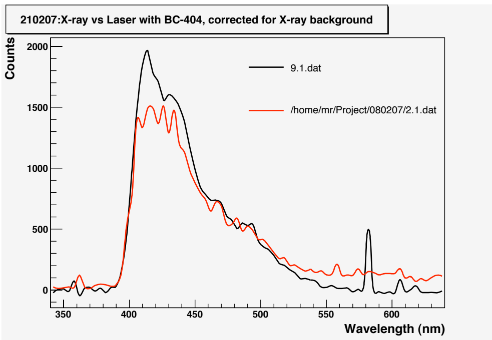

(a) 4nm bins.

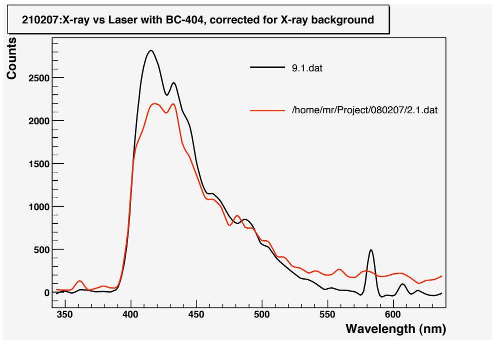

(b) 6 nm bins.

Figure 35: BC-404: Smoothing of X-ray and Laser spectra by Rebinning.

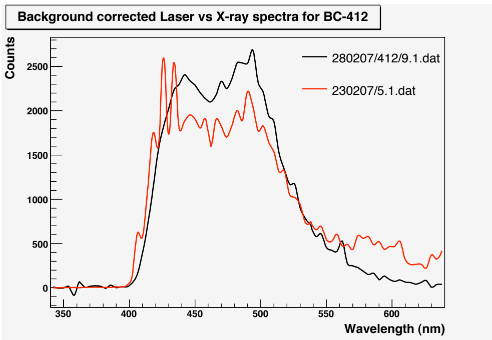

(a) 4nm bins.

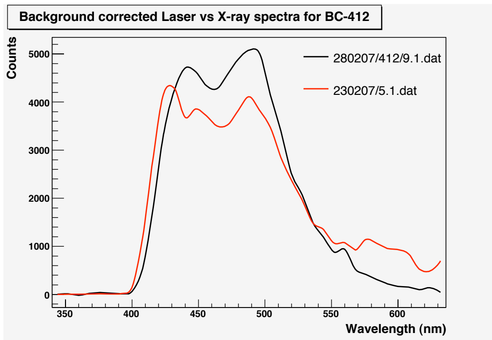

(b) 6 nm bins.

Figure 36: BC-412: Smoothing of X-ray and Laser spectra by Rebinning.

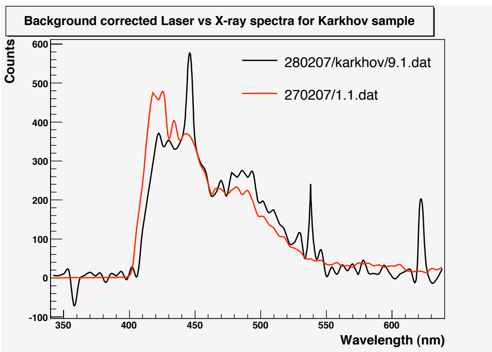

(a) 4nm bins.

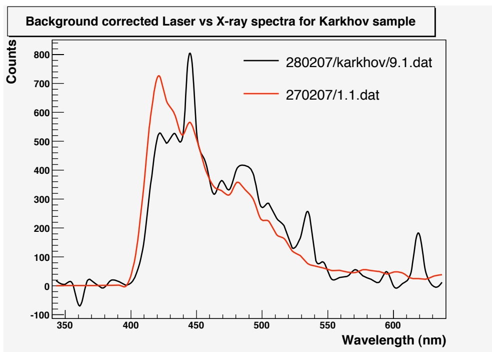

(b) 6 nm bins.

Figure 37: Karkhov sample: Smoothing of X-ray and Laser spectra by Rebinning.

D OOIBase32 Output File

This is the beginning and end of the first `.Scope` file that was produced from OOIBase32, `Samplespectra.00000001.Master.Scope`, with most of the numerical data omitted:

```
   OOIBase32 Version 2.0.6.5 Data File
++++++++++++++++++++++++++++++++++++
Date: 11-10-2006, 11:35:05
User: Matthew Rose
Spectrometer Serial Number: USB2E4595
Spectrometer Channel: Master
Integration Time (msec): 300
Spectra Averaged: 0
Boxcar Smoothing: 0
Correct for Electrical Dark: Enabled
Time Normalized: Disabled
Dual-beam Reference: Disabled
Reference Channel: Master
Temperature: Not acquired
Spectrometer Type: S2000
ADC Type: USB2000
Number of Pixels in File: 2048
Graph Title:
>>>>>Begin Spectral Data<<<<<
339.98 0.000
340.35 0.000
340.72 -5.853
.       .
.       .
.       .
1013.42 -5.171
1013.70 1.147
1013.98 1.829
>>>>>End Spectral Data<<<<<
```

All header lines were removed to produce `roombackground1.dat`, as described in section 3.1.1.

E Macros for use in root.

E.1 ledmacro2.cxx

The first working macro, written using the ROOT[22] tutorials:

```
   {
//   example of macro to read data from an ascii
//  file and create a root file with an histogram
//  and an ntuple.
   gROOT->Reset();
#include "Riostream.h"

   ifstream in;
// we assume a .dat file in the current directory
// this file has 2 columns of float data, the path
//is entered below
   in.open("ascii3.dat");

   Float_t x,y;
   Int_t nlines = 0;

   TFile *f = new TFile("ledspectrum.root","RECREATE");
   TH1F *h1 = new TH1F("h1","LED Test Spectrum",1200,
340,640);
   TNtuple *ntuple = new TNtuple("ntuple","data from
ascii file","x:y");

   while (1) {
      in >> x >> y;
  //cout << x << "  " << y << endl;
      if (!in.good()) break;
h1->Fill(x,y);
      //ntuple->Fill(x,y);
      nlines++;
   }
   printf(" found %d points",nlines);

   in.close();
   f->Write();
   h1->Draw();
}
```

E.2 `tinymacro.cxx`

This was developed from `ledmacro.cxx`, removing all superfluous lines:

```
   {
   gROOT->Reset();
#include "Riostream.h"
   ifstream in;
   in.open("/Project/autumnlaser/laseronly.1.dat");
   Float_t x,y;
   Int_t nlines = 0;
   TH1F *h1 = new TH1F("h1","Laser Test Spectrum",
1200,340,640);
   while (1) {
      in >> x >> y;
      if (!in.good()) break;
h1->Fill(x,y);
      nlines++;
   }
   in.close();
   h1->Draw();
}
```

E.3 `unscaled5datswback.cxx`

This macro produces one canvas with 5 unscaled spectra, and a background reading. It was used to produce Figures 16c and 16d.

```
   {
//   macro to read data from an ascii file
//   and create a number of histograms
gROOT->Reset();
#include "Riostream.h"

char file1[50];
char file2[50];
char file3[50];
char file4[50];
char file5[50];
char fileb[50];
Double_t max = 640.0;
Double_t min = 340.0;
```

```
//bin chosen to remove lines to zero, giving a nicer plot
Int_t bin = 150;
//Int_t bin = 2048;
Int_t choice = 5;
Int_t option = 5;
ifstream in;
ifstream in2;
ifstream in3;
ifstream in4;
ifstream in5;
ifstream inb;
//char files[100];
// we assume a file *.dat in the current directory
// this file has 2 columns of float data.

printf("Which File (1)?\n");
scanf("%s", file1);
printf("Which File (2)?\n");
scanf("%s", file2);
printf("Which File (3)?\n");
scanf("%s", file3);
printf("Which File (4)?\n");
scanf("%s", file4);
printf("Which File (5)?\n");
scanf("%s", file5);
printf("Which background file (6)?\n");
scanf("%s", fileb);

c1 = new TCanvas("c1","c1",640,480);

TH1F *h1 = new TH1F("h1",file1,bin,min,max);
h1->SetXTitle("Wavelength (nm)");
h1->SetLabelSize(0.03,"x");
h1->SetYTitle("Counts");
h1->SetLabelSize(0.03,"y");
h1->SetLineColor(8);
h1.GetYaxis()->SetTitleOffset(1.31);
in.open(file1);
Float_t x,y;
Int_t nlines = 0;
while (1) {
```

```
  in >> x >> y;
  if (!in.good()) break;
  h1->Fill(x,y);
  nlines++;
}
in.close();

TH1F *h2 = new TH1F("h2",file2,bin,min,max);
in2.open(file2);
Float_t x2,y2;
Int_t nlines2 = 0;
while (2) {
  in2 >> x2 >> y2;
  if (!in2.good()) break;
  h2->Fill(x2,y2);
  nlines2++;
}
in2.close();

TH1F *h3 = new TH1F("h3",file3,bin,min,max);
in3.open(file3);
Float_t x3,y3;
Int_t nlines3 = 0;
while (3) {
    in3 >> x3 >> y3;
    if (!in3.good()) break;
    h3->Fill(x3,y3);
    nlines3++;
  }
in3.close();


TH1F *h4 = new TH1F("h4",file4,bin,min,max);
in4.open(file4);
Float_t x4,y4;
Int_t nlines4 = 0;
while (4) {
    in4 >> x4 >> y4;
    if (!in4.good()) break;
    h4->Fill(x4,y4);
    nlines4++;
```

```
  }
in4.close();


TH1F *h5 = new TH1F("h5",file5,bin,min,max);
in5.open(file5);
Float_t x5,y5;
Int_t nlines5 = 0;
while (5) {
    in5 >> x5 >> y5;
    if (!in5.good()) break;
    h5->Fill(x5,y5);
    nlines5++;
  }
in5.close();

TH1F *hb = new TH1F("hb",fileb,bin,min,max);
inb.open(fileb);
Float_t xb,yb;
Int_t nlinesb = 0;
while (5) {
    inb >> xb >> yb;
    if (!inb.good()) break;
    hb->Fill(xb,yb);
    nlinesb++;
  }
inb.close();
/*
//normalise the histograms by scaling so that integral = 1
TH1F *h1n = (TH1F*) h1->Clone();
h1n->SetName("h1n");
TH1F *h2n = (TH1F*) h2->Clone();
h2n->SetName("h2n");
TH1F *h3n = (TH1F*) h3->Clone();
h3n->SetName("h3n");
TH1F *h4n = (TH1F*) h4->Clone();
h4n->SetName("h4n");
TH1F *h5n = (TH1F*) h5->Clone();
h5n->SetName("h5n");
Double_t scale2 = (h1->Integral())/(h2->Integral());
h2n->Scale(scale2);
```

```
Double_t scale3 = (h1->Integral())/(h3->Integral());
h3n->Scale(scale3);
Double_t scale4 = (h1->Integral())/(h4->Integral());
h4n->Scale(scale4);
Double_t scale5 = (h1->Integral())/(h5->Integral());
h5n->Scale(scale5);
//create duplicate of h1, hcheat,
//in order to manipulate title etc.

*/TH1F *hcheat = (TH1F*) h1->Clone();
hcheat->SetName("overlay");
hcheat->SetTitle("230207:BC-412 Laser spectra, unscaled with
background reading");
//plot normalised h1 & h2 on c3
hcheat->Draw();

h1->Draw("histsame");
h2->Draw("histsame");
h3->Draw("histsame");
h4->Draw("histsame");
h5->Draw("histsame");
hb->Draw("histsame");
h1->SetLineColor(1);
h2->SetLineColor(2);
h3->SetLineColor(4);
h4->SetLineColor(7);
h5->SetLineColor(8);
hb->SetLineColor(6);
hcheat->SetLineColor(1);
//add a legend
leg_hist = new TLegend(0.6,0.7,0.89,0.89);
leg_hist->AddEntry(h1,file1,"l");
leg_hist->AddEntry(h2,file2,"l");
leg_hist->AddEntry(h3,file3,"l");
leg_hist->AddEntry(h4,file4,"l");
leg_hist->AddEntry(h5,file5,"l");
leg_hist->AddEntry(hb,fileb,"l");
leg_hist->Draw();
c1->Modified();
}
```

E.4 `backgroundsubtractionfor5dats.cxx`

This macro produces two canvases, one showing 5 raw spectra and the background reading, and one showing the 5 spectra after the background reading has been subtracted, scaled to have the same integral. The spectra in Figures 26- 28 were produced using this macro.

```
   {
//   macro to read data from an ascii file
//   and create a number of histograms
gROOT->Reset();
#include "Riostream.h"

char file1[50];
char file2[50];
char file3[50];
char file4[50];
char file5[50];
char file6[50];
Double_t max = 640.0;
Double_t min = 340.0;
Int_t bin = 150;
ifstream in;
ifstream in2;
ifstream in3;
ifstream in4;
ifstream in5;
ifstream in6;
// we assume a file *.dat in the current directory
// this file has 2 columns of float data.

printf("Which File (1)?\n");
scanf("%s", file1);
printf("Which background file?\n");
scanf("%s", file2);
printf("Which File (2)?\n");
scanf("%s", file3);
printf("Which File (3)?\n");
scanf("%s", file4);
printf("Which File (4)?\n");
scanf("%s", file5);
printf("Which File (5)?\n");
```

```
scanf("%s", file6);

in.open(file1);
Float_t x,y;
Int_t nlines = 0;

// create canvas c1 and histogram h1,
// set bins, xmax, xmin
c1 = new TCanvas("c1","c1",384,288);
TH1F *h1 = new TH1F("h1","5dats & background",bin,min,max);

// set axis titles and styles, established by
// experimenting within canvas
h1->SetXTitle("Wavelength (nm)");
h1->SetLabelSize(0.03,"x");
h1->SetYTitle("Counts");
h1->SetLabelSize(0.03,"y");
//h1->SetLineColor(1);
h1.GetYaxis()->SetTitleOffset(1.31);


while (1) {
    in >> x >> y;
    if (!in.good()) break;
    h1->Fill(x,y);
    nlines++;
  }
in.close();
h1->Draw();


in2.open(file2);
Float_t x2,y2;
Int_t nlines2 = 0;
TH1F *h2 = new TH1F("h2",file2,bin,min,max);
h2->SetLineColor(28);
while (2) {
  in2 >> x2 >> y2;
  if (!in2.good()) break;
  h2->Fill(x2,y2);
  nlines2++;
```

```
}
in2.close();
h2->Draw("histsame");


in3.open(file3);
Float_t x3,y3;
Int_t nlines3 = 0;
TH1F *h3 = new TH1F("h3",file3,bin,min,max);
h3->SetLineColor(2);
while (3) {
  in3 >> x3 >> y3;
  if (!in3.good()) break;
  h3->Fill(x3,y3);
  nlines3++;
}
in3.close();
h3->Draw("histsame");

in4.open(file4);
Float_t x4,y4;
Int_t nlines4 = 0;
TH1F *h4 = new TH1F("h4",file4,bin,min,max);
h4->SetLineColor(4);
while (4) {
  in4 >> x4 >> y4;
  if (!in4.good()) break;
  h4->Fill(x4,y4);
  nlines4++;
}
in4.close();
h4->Draw("histsame");

in5.open(file5);
Float_t x5,y5;
Int_t nlines5 = 0;
TH1F *h5 = new TH1F("h5",file5,bin,min,max);
h5->SetLineColor(6);
while (5) {
  in5 >> x5 >> y5;
  if (!in5.good()) break;
```

```
  h5->Fill(x5,y5);
  nlines5++;
}
in5.close();
h5->Draw("histsame");

in6.open(file6);
Float_t x6,y6;
Int_t nlines6 = 0;
TH1F *h6 = new TH1F("h6",file6,bin,min,max);
h6->SetLineColor(8);
while (6) {
  in6 >> x6 >> y6;
  if (!in6.good()) break;
  h6->Fill(x6,y6);
  nlines6++;
}
in6.close();
h6->Draw("histsame");

legendary = new TLegend(0.6,0.7,0.89,0.89);
legendary->AddEntry(h1,file1,"l");
legendary->AddEntry(h3,file3,"l");
legendary->AddEntry(h4,file4,"l");
legendary->AddEntry(h5,file5,"l");
legendary->AddEntry(h6,file6,"l");
legendary->AddEntry(h2,"background","l");
legendary->Draw();
c1->Modified();

c2 = new TCanvas("c2","c2",640,480);

TH1F *hx1 = new TH1F("hx","5dats-background",bin,min,max);
hx1->Add(h1,h2,1,-1);
hx1->SetXTitle("Wavelength (nm)");
hx1->SetLabelSize(0.03,"x2");
hx1->SetYTitle("Counts");
hx1->SetLabelSize(0.03,"y2");
hx1.GetYaxis()->SetTitleOffset(1.31);
//hx1->setLineColor(1);
hx1->Draw();
```

```
TH1F *hx3 = new TH1F("hx3","hx3",bin,min,max);
hx3->Add(h3,h2,1,-1);
TH1F *hx4 = new TH1F("hx4","hx4",bin,min,max);
hx4->Add(h4,h2,1,-1);
TH1F *hx4 = new TH1F("hx5","hx5",bin,min,max);
hx5->Add(h5,h2,1,-1);
TH1F *hx6 = new TH1F("hx6","hx6",bin,min,max);
hx6->Add(h6,h2,1,-1);

TH1F *h3s = (TH1F*) hx3->Clone();
h3s->SetName("h3s");
Double_t scale = (hx1->Integral())/(hx3->Integral());
h3s->Scale(scale);
h3s->SetLineColor(2);
h3s->Draw("histsame");

TH1F *h4s = (TH1F*) hx4->Clone();
h4s->SetName("h4s");
Double_t scale = (hx1->Integral())/(hx4->Integral());
h4s->Scale(scale);
h4s->SetLineColor(4);
h4s->Draw("histsame");

TH1F *h5s = (TH1F*) hx5->Clone();
h5s->SetName("h5s");
Double_t scale = (hx1->Integral())/(hx5->Integral());
h5s->Scale(scale);
h5s->SetLineColor(6);
h5s->Draw("histsame");

TH1F *h6s = (TH1F*) hx6->Clone();
h6s->SetName("h6s");
Double_t scale = (hx1->Integral())/(hx6->Integral());
h6s->Scale(scale);
h6s->SetLineColor(8);
h6s->Draw("histsame");

leg_hist = new TLegend(0.6,0.7,0.89,0.89);
leg_hist->AddEntry(hx1,file1,"l");
leg_hist->AddEntry(h3s,file3,"l");
leg_hist->AddEntry(h4s,file4,"l");
```

```
leg_hist->AddEntry(h5s,file5,"l");
leg_hist->AddEntry(h6s,file6,"l");
leg_hist->Draw();
c2->Modified();

}
```